Indian Journal of Biochemistry & Biophysics
Vol. 62, December 2025, pp. 1325-1350
DOI: 10.56042/ijbb.v62i12.17913

Quantum chemical analysis and anticancer evaluation of 1, 4-benzenedicarboxylic acid bis (2-ethylhexyl) ester: Topological indices, reduced density gradient, molecular electrostatic potential, natural bond orbital

S Kayashrini[1], P Rajesh[1]*, E Dhanalakshmi[1], M Anbarasu[2], M Kesavan[3], M Prabhaharan[4], R Mohamed Hisam[1] & R Sudha[5]

[1]Department of Physics, School of Basic Sciences; [2]Department of Agronomy, School of Agriculture; & [5]Department of Chemistry, Vels Institute of Science, Technology & Advanced Studies (VISTAS), Pallavaram, Chennai-600 117, Tamil Nadu, India

[3]Interdisciplinary Institute of Indian System of Medicine, SRM Institute of Science and Technology, Kattankulathur, Chennai-603 203, Tamil Nadu, India

[4]Department of Physics, Saveetha School of Engineering, Saveetha Institute of Medical and Technical Sciences (SIMATS), Chennai-602 105, Tamil Nadu, India

Received 14 March 2025; *revised 13 May 2025*

Liver cancer remains one of the most lethal malignancies worldwide, highlighting the urgent need for improved treatment strategies. This study employed density functional theory (DFT) quantum calculations and molecular docking studies to evaluate the specificity and anticancer potential of therapeutic compounds derived from *Hybanthus enneaspermus*. The investigation focused on the interaction of 1, 4-Benzenedicarboxylic Acid, Bis (2-Ethylhexyl) Ester (4B2EH) with specific active methylene reagents and hydrogen nucleophiles. Global reactivity descriptors were utilized to assess the compound's molecular stability and reactivity against liver cancer. Compounds extracted through the Soxhlet technique were further confirmed using spectroscopic methods, including FT-IR, ^{1}H NMR, ^{13}C NMR, GC-MS, and UV-Vis analyses. The electronic properties of 4B2EH were examined using the DFT/B3LYP/6-311++G (d, p) functional, employing time-dependent density functional theory (TD-DFT) for advanced insights. The study utilized Veda 04 software for PED values, alongside Gaussian 09W, Gauss View 6.0, and ChemCraft 1.8 for comprehensive molecular visualization and analysis. The investigation focused on key aspects such as the MEP surface, HOMO-LUMO analysis, and NBO interactions, specifically C4 – C5 (π) → C10 – O11 (π^*) and $\pi \rightarrow \pi^*$ transitions. Additionally, DOS, RDG, ELF, and LOL analyses were conducted to predict the compound's stability, anticancer potential, and reactive sites for electrophilic and nucleophilic attacks. Furthermore, molecular docking simulations were performed against two distinct protein receptors (PDB ID: 2H80 and 9ETE) to evaluate binding conformations and interaction profiles with key liver cancer targets. The simulations revealed binding energies of -5.08 kcal/mol and -5.83 kcal/mol, indicating favourable interactions and potential therapeutic applications. Additionally, topological indices such as the 58.24 RR index, 5.87 RA index, and 5.89 S index demonstrated strong correlations with key molecular properties. These indices, combined with factors like polarity surface area and docking scores, play a crucial role in identifying potential lead compounds for drug development. The analysis highlights essential chemical attributes, biological activity, and other relevant data obtained through degree-based QSPR analysis.

Keywords: 4B2ES, FT-IR, Molecular Docking, QSPR analysis, UV-Vis

There are many new inventions and ailments in the modern world, and a significant portion of medicine has been developed to treat them. The World Health Organization (WHO) and the National Library of Medicine claim that cancer is currently the most common and prevalent disease. Due to negligence and a lack of knowledge, there is a significant deficiency in the identification of different malignancies, which can lead to a high death rate. With an expected 905, 677 new cases and 830, 180 fatalities from the disease in 2020, primary liver cancer (PLC) ranks third globally in terms of cancer-related mortality and is the sixth most prevalent kind of cancer diagnosed. Many people with fatty livers are affected by stress, drugs, and alcohol addiction, which causes liver damage and liver cancer in the population with pollution. The known cause of cancer is the unknown factor behind the scenarios with various drugs and compounds involved to rectify the gap in treatment and the drug designing and used to decrease the risk factor of death in the world. With over 866, 000 new

*Correspondence:
E-mail: rajesh.ncc5coy@gmail.com

cases and around 760, 000 fatalities each year, liver cancer is still a major worldwide health problem in 2024. Hepatocellular carcinoma, or HCC, accounts for 74.5% of instances worldwide and is most common in areas such as sub-Saharan Africa, Eastern Asia, and portions of Southeast Asia. While intrahepatic cholangiocarcinoma (ICCA) is more prevalent in places like Northern Africa and Europe, a larger percentage of HCC is seen in men and younger people. Hepatitis B and C infections, alcohol-induced liver damage, and non-alcoholic steatohepatitis (NASH) all have a significant impact on the prevalence of liver cancer[1]. An ethnobotanical plant that is widely utilized in Indian traditional medicine is *Hybanthus enneaspermus*, according to the literature review. OrilaiThamarai, in Tamil, Munbora in Bengali English: Flower of the Spade Ratan Purush in Hindi, there are distinct names for Kannada (Parsvanatha) and Malayalam (Orilathamata) in different places. It belongs to the Violaceae family of flowering plants. Men are said to benefit greatly from this plant, which is used as a tonic, diuretic, and demulcent. As a diuretic, the root is used to treat digestive problems and urinary diseases in youngsters. The fruit is used to relieve scorpion stings[2]. The plant contains a variety of phytocompounds, including sugars, tannins, alkaloids, dipeptide, isoarborinol, sitosterol, and flavonoids. Recent studies have demonstrated the plant's therapeutic properties against a variety of terrible illnesses.The fruit has antivenomous properties that protect against scorpion and snake stings. It is used in Siddha medicine to encourage mothers to secrete more milk. It is used to treat illnesses connected to stress and boosts libido. Antifungal, antibacterial, antiviral, antioxidant, neuroprotective, cardioprotective, anti-arthritic, antinociceptive, antiallergic, anticonvulsant, antihyperlipidemic, and nephroprotective properties are among its many actions[3]. 4B2EH, often referred to as dioctyl terephthalate (DOTP), terephthalic acid, or diisobutyl ester, is a regularly used non-phthalate plasticizer, according to the literature review. It is a transparent, colorless, or pale-yellow liquid that is an ester made from terephthalic acid and 2-ethylhexanol[4]. Because of its low toxicity, 4B2ES is a popular option for products that need safe and environmentally friendly materials, like toys for kids, medical equipment, and food packaging. 4B2EH is primarily used as a plasticizer in flexible PVC products, such as cables, flooring, and artificial leather, where it improves flexibility, heat resistance, and durability. It is also used in adhesives, sealants, and coatings, which further expands its versatility. With a density of roughly 0.985 g/cm³ at 20°C and a boiling point of about 386°C, 4B2EH demonstrates excellent performance characteristics, such as low volatility and compatibility with a variety of polymers, making it a crucial component of both consumer and industrial goods. As far as I'm aware, nobody is capable of doing this task. To confirm the compound and forecast the effectiveness of the application findings, the purpose of this study is to look into the anticancer activity, specifically for liver cancer, that can be achieved through this compound using the DFT studies by subjecting it to GC-MS analysis along with UV-Vi's analysis, FT-IR analysis, and NMR studies. Using the B3LYP/6-311++G (d, p) basis and DFT calculations, the studies' ELF, LOL and RDG analysis provide a fuller explanation of the physical and chemical characteristics with optimized structure, while NBO and HOMO-LUMO provide geometrical attributes.To design analyte-specific receptors and determine the compound 4B2EH capacity through docking studies using Autodock 4.0 the scientific community must concentrate on developing new anticancer compounds or improving those that are already available from natural sources. In addition to the mathematical studies that are incorporated to clarify the 4B2EH, the anticancer activity of liver cancer will be corrected to create a cleaner and healthier environment.

Methodology of 4B2EH

Hybanthus enneaspermus green synthesis

In India, Tamil Nadu, Thanjavur district, Athivette hamlet is where the *Hybanthus enneaspermus* was harvested. Three kilograms of *Hybanthus enneaspermus*, a 100% medicinal plant, were cleaned with fresh water and allowed to dry in a shade dry condition for 25 to 30 days at room temperature. Additionally, 1 kg of the conserved section was ground into a fine powder and mixed with 95.5% methanal (2:1), which was then left at room temperature for 48 h to monitor the constituents. Leaf extract was filtered using Whatman filter paper for qualitative analysis, and crude and methanol was separated using the Soxhlet method and rotary evaporator procedure[5].

Experimental Details

The crude was examining the Shimadzu QP2010 Plus gas chromatography-mass spectrometry (GC-MS) method. With dimensions of 30 m in length, 0.25 mm in inner diameter, and 0.25 m in thickness, the polydimethylsiloxane-coated MS non-polar capillary column is utilized for injection at temperatures ranging from 4 to 450°C. The GC-MS spectra show a region of 25 minutes with an advanced flow controller controlling the carrier gas using detectors such as FID, BID, TCD, ECD, and MS. The powdered pharmaceutical medication molecule 4B2ES was purchased from Sigma-Aldrich, a reputable chemical manufacturer, and utilized straight away without any additional purification. The sophisticated and precise equipment used in UV-visible spectroscopy allows for precise material analysis based on light absorption characteristics. The light source, which is typically a deuterium lamp for the UV region and a tungsten-halogen lamp for the visible spectrum, emits a continuous spectrum of light. Using a Perkin Elmer-Lambda 35 UV Win lab V6.0 Spectrometer at normal temperature, the Ultra Violet-Visible absorption spectra were investigated in the wide wavelength range of 185-3300 nm, with a variable bandwidth of 0.5e4.0 nm. UV-3600+ Shimadzu Instrument uses a Varian Cary 5E-UV-NIR Spectrometer with a quartz cell that has a diameter of 1 cm and a slit width of 0.5 nm[6]. Using a KBr pellet method with a 4 cm^{-1} resolution, a PERKIN ELMER FT-IR Spectrometer with a high speed of 20 spectra per second, and a sensitivity at a S/N ratio of 60000:1, the TTCPE sample was evaluated using FT-IR spectrum analysis in the recorded area in the region 7800-350 cm^{-1}. Using CDCl3 at 25°C, NMR studies were conducted on a Varian Mercury Plus NMR spectrometer running at 500 MHz.Tramethylsilane (TMS) was used as an internal reference for the 1H and 13C NMR spectra, which were recorded at 300 K on a Bruker high-solution nuclear magnetic resonance spectrometer. TMS (d¼ 0.00 ppm) and CDCl3 (d¼77.00 ppm) were used as internal standards, and chemical shifts were reported in parts per million (ppm). Varian standard pulse sequences were used for 1H, 13C, gradient heteronuclear single quantum correlation spectroscopy (gHSQC), gradient heteronuclear multiple bond correlation spectroscopy (gHMBC), and gradient double quantum-filtered correlation spectroscopy (gDQCOSY). The glass tube is 0.3 cm in diameter and 8.5 cm long. At 60–100 MHZ, it aids in producing a uniform magnetic field. HMBC HMQC DQ FCOSY & TOCSY 2D NMR (COSY HSQC). In Kattankulathur, Chengalpattu district, Tamil Nadu, India, NMR spectra were obtained at the SRM College of Science using a base frequency of 400 MHz for 1H nuclei and 100 MHz for 13C nuclei (4:1 ratio) [7].

Computational details

The Gaussian 09 W program was used for all theoretical calculations. In the computational analysis of the 4B2EH molecular structure, the geometry parameters of bond angle and bond length, HOMO-LUMO, and MEP were represented using Gauss View 6.0 and ChemCraft 1.8 tools. The reactive site was located using the MEP surface, Mulliken population analysis, NMR, electronic characteristics of the energy gap, electrophilicity index, and nucleophilicity index. Using the hybrid functional Becke-3-Lee–Yang–Parr (B3LYP) parallel with 6-311++G (d.p) program, the results were interpreted using the DFT approach[8]. The vibrational wave number of FT-IR spectra corresponding to PED% was determined using Veda 04 software, and the findings demonstrate a strong connection with the experiment spectra. The calculated UV-visible absorption spectra with the gas and several solvents were analyzed using the TD-DFT technique. The natural bond orbital investigation (hyperconjugation contact, donor-acceptor charge transfer, and intramolecular hydrogen-bonding interaction), antibonding, and high stabilization energy values are interpreted by second-order perturbation theory, which is carried out using Gaussian 09 W software. RDG, ELF, and LOL topological parameters have been computed using the MULTIWFN 3.7 bin Win 64 application. In the molecular docking study, the ligand-protein interaction and receptor binding were computed using the tool Autodock 4.0 software[9].

Results and Discussion

GC-MS analysis

The *Hybanthus enneaspermus* samples that were isolated from the whole plant were analyzed by Shimadzu utilizing GC-MS QP 2010.It may contain a mixture of various phytochemicals, including both volatile and non-volatile components. To prepare the sample for GC-MS analysis, we followed a standard protocol as reported in the literature review[10]. One milligram of the extracted sample was combined with

1 ml of methanol as a solvent to prepare the sample to eliminate excessive methanol, the extract was first concentrated using a rotary evaporator. After filtering and re-dissolving in methanol, the concentrated sample was added to the GC-MS apparatus. To inject the sample into the Zebron ZB-FFAP column fused with silica, the devices had a split mode injector. The 60 m × 0.25 mm column has a separation film thickness of 0.25 µm. The flow rate of helium as a carrier gas was 1 milliliter per minute. At a rate of 1 µl/min, the sample was injected in a split mode with a split ratio of 1:50. At 250°C, the injection temperature was kept constant. A pressure of 53.5 kPa, an interface temperature of 280°C, and an ion source temperature of 200°C, are additional prerequisites for GC-MS operation. The column oven was kept at 50°C for 1 min, and then its temperature was gradually increased by 10°C per minute until it reached 280°C, where it stayed for two minutes. The GC-MS scan spectra have a range width of 40–700 *m/z*. The Wiley 8 and NIST 14 libraries included with the GC-MS equipment were used to identify the components by comparing their retention indices. The computer libraries (Wiley 8 and NIST 14) were used to tabulate the components that were found. Based on the quantitative phytochemical compound 4B2ES's anti-cancer efficacy, the GC-MS result identified a bio-compound for more research. The 4B2EH GC-MS data is displayed in (Fig.1). Gas chromatography-mass spectrometry study of the *Hybanthus enneaspermus* methanol extract revealed 4B2EH, which is associated with a retention time of 40.81 minutes and a molecular weight of 390 g/mol with the formula C24H38O4. These bio-components have been discovered, and the NIST data library and PubChem databases have the corresponding information. The 4B2EH molecule was the subject of comparative investigations on molecular docking, spectroscopic analysis, and quantum chemical computation, respectively.

Optimized Structure

Together with the chemical structure and 4B2EH numbering, the molecule's optimal molecular geometry is shown in (Fig. 2). The Gaussian 09, which is programmed using the DFT/B3LYP technique with the 6-311++G (d, p) basis set, is used to find geometrical features like as bond length and

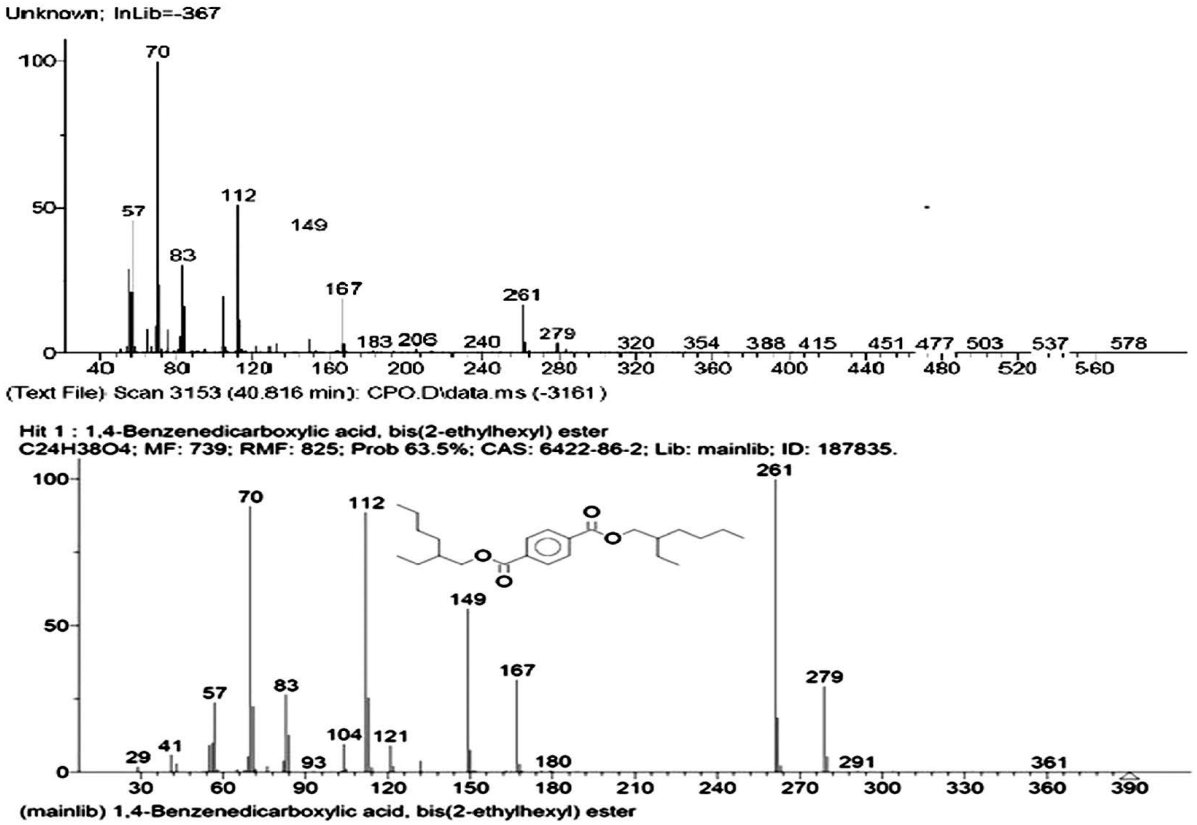

Fig.1 — GC-MS of a 4B2EH

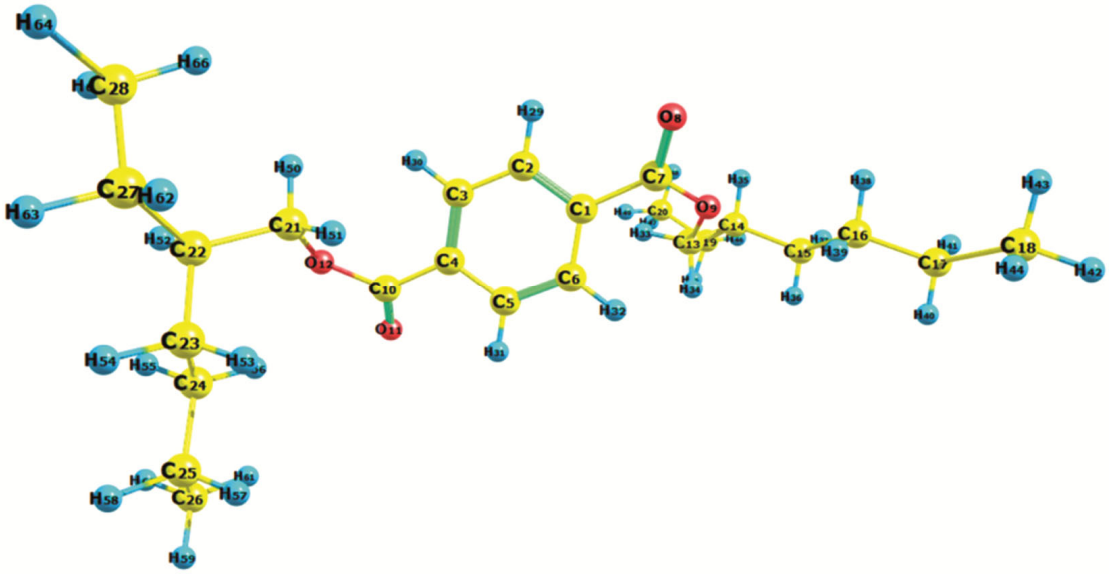

Fig.2 — Optimized structure of the 4B2EH

bond angle. The optimized structural parameters that match the experimentally observed XRD data are displayed in (Fig. 2) [11]. 4B2EH is an organic chemical that is sometimes referred to as dioctyl terephthalate (DOTP). Characteristics of 4B2EH where, Formula for the chemical: C24H38O4 Weight in molecules: 390.56 g/mol, Liquid appearance: clear, colourless, or faintly yellow. The boiling point is around 400°C. Odor: subtle, Point of Melting: <-50°C Density at 20°C: about 0.98 g/cm³ Viscosity: moderate; temperature-dependent 210°C is the flash point (open cup technique). Solubility: Water is insoluble It dissolves in organic solvents like ethers, ketones, and alcohols. Storage: Keep away from potent oxidizers and in a cold, drylocation.A benzene ring with two carboxylate ester groups joined to the 1 and 4 locations, each of which has a 2-ethylhexyl chain, makes up the structural distribution of the 4B2EH molecule. Most likely, it would result from structural alterations or conjugation with bioactive groups intended to disrupt the pathways of cancer cells[12]. Mechanisms such as DNA intercalation, enzyme inhibition, or apoptosis induction may be involved. Together with the benzene ring and the coo groups attached at the corner position; the di carbocyclic group found in compound 4B2EH represents the primary game-changing structure for all applications to break the studied material more deeply. Additionally, the bis ethelhexyl is present in the hanking position to the coo groups on both sides of the benzene structure. The Bond Angle and Bond Length are part of the structure's optimal molecular geometry, as shown in (Table 1). There are C1, C2, C3, C4, C5, C6, H30, H29, H32, and H31 in the benzene structure. The existence of several groups that reflect the linear, planer, and nonlinear combinations of the 4B2ES is defined by the carbocyclic group, which includes the C1, C7, O8, O9, and C4, as well as the 2-ethelhexyl remaining C and H groups. The connection between the CCC, HCH, CCO, OCO, CHC, HHC, and CCH with maximum and minimum values that correspond to the experimental XRD values is also described by the combination of the CC, CH, CH2, CH3, and COO of bond length and bond angle obtained in this title compound[13]. The bond lengths of the double were C1-C2 = 1.401/1.406, C3-C4 = 1.4021/1.089, C5-C6 = 1.3909/1.369, C13-C14 = 1.5339/1.530, C10-O11 = 1.2118/1.218, and C7-O8 = 1.2101/1.271. These were closely correlated with the experimental parameters that reached the compound's C=C and C-C bonds with the highest bond angle. Among the values and the elemental representation of the single bonded values were C21-C22=1.5318/ 1.498, C1-C7=1.5026/1.501, C10-O12=1.356/1.308, C7-O9=1.3574/1.373, C2-C1-C6=119.3818/119.3, C2-C1-C7=117.8767/118.9, C6-C1-C7=122.5479/121.2, C1-C2- C3=120.3712/119.9, C2-C3-C4=120.245/121.5, C3-C4-C5=119.3681/117.8, C3-C4-C10=122.8004/123. 41, C5-C4-C10=117.6678/117.34, C4-C5-C6=120.3811/ 119.46, C1-C6-C5=120.2443/120.4, C9-C13-C14= 109.6773/109.9, C13-C14-C15=113.1073/116.6, C21-C22-C23=112.8264/113.4. The values of the double

Table 1 — Structural parameter of the 4B2EH

Bond Length (Å)	B3LYP/6–311G (d, p)	Experimental* [12]	Bond Angle (◦)	B3LYP/6–311G (d, p)	Experimental* [13]
C_1-C_2	1.401	1.406	C_{14}-C_{13}-H_{33}	110.9577	109.7
C_1-C_6	1.4021	1.405	C_{14}-C_{13}-H_{34}	109.9977	109.7
C_1-C_7	1.5026	1.501	H_{33}-C_{13}-H_{34}	108.0384	107.7
C_2-C_3	1.3911	1.380	C_{13}-C_{14}-C_{15}	113.1073	116.6
C_2-H_{29}	1.0846	1.030	C_{13}-C_{14}-C_{19}	109.5508	-
C_3-C_4	1.4021	1.089	C_{13}-C_{14}-H_{35}	106.9718	-
C_3-H_{30}	1.0845	1.030	C_{15}-C_{14}-C_{19}	110.0666	-
C_4-C_5	1.4012	1.391	C_{15}-C_{14}-H_{35}	108.7104	-
C_4-C_{10}	1.5016	1.507	C_{19}-C_{14}-H_{35}	108.2773	-
C_5-C_6	1.3909	1.369	C_{14}-C_{15}-C_{16}	117.0926	117.8
C_5-H_{31}	1.0845	1.031	C_{14}-C_{15}-H_{36}	108.4486	-
C_6-H_{32}	1.0846	1.022	C_{14}-C_{15}-H_{37}	107.512	-
C_7-O_8	1.2101	1.271	C_{16}-C_{15}-H_{36}	109.2676	-
C_7-O_9	1.3574	1.373	C_{16}-C_{15}-H_{37}	108.3368	-
O_9-C_{13}	1.4475	1.244	H_{36}-C_{15}-H_{37}	105.5774	107.7
C_{10}-O_{11}	1.2118	1.218	C_{15}-C_{16}-C_{17}	112.4241	113.7
C_{10}-O_{12}	1.356	1.308	C_{15}-C_{16}-H_{38}	109.4204	-
O_{12}-C_{21}	1.4464	1.447	C_{15}-C_{16}-H_{39}	110.3525	-
C_{13}-C_{14}	1.5339	1.530	C_{17}-C_{16}-H_{38}	109.4385	-
C_{13}-H_{33}	1.0923	1.010	C_{17}-C_{16}-H_{39}	109.403	-
C_{13}-H_{34}	1.097	1.010	H_{38}-C_{16}-H_{39}	105.5701	108.2
C_{14}-C_{15}	1.543	1.400	C_{16}-C_{17}-C_{18}	113.1171	-
C_{14}-C_{19}	1.5471	1.474	C_{16}-C_{17}-H_{40}	109.3043	-
C_{14}-H_{35}	1.0992	0.930	C_{16}-C_{17}-H_{41}	109.3788	-
C_{15}-C_{16}	1.5354	1.470	C_{18}-C_{17}-H_{40}	109.4082	-
C_{15}- H_{36}	1.101	0.930	C_{18}-C_{17}-H_{41}	109.4734	-
C_{15}-H_{37}	1.0987	0.930	H_{40}-C_{17}-H_{41}	105.9048	-
C_{16}-C_{17}	1.5342	1.377	C_{17}-C_{18}-H_{42}	111.4958	-
C_{16}-H_{38}	1.0983	0.980	C_{17}-C_{18}-H_{43}	111.1767	-
C_{16}-H_{39}	1.0953	0.970	C_{17}-C_{18}-H_{44}	111.1569	-
C_{17}-C_{18}	1.5316	1.410	H_{42}-C_{18}-H_{43}	107.7045	108.2
C_{17}-H_{40}	1.099	0.930	H_{42}-C_{18}-H_{44}	107.7169	107.7
C_{17}-H_{41}	1.0988	0.970	H_{43}-C_{18}-H_{44}	107.3989	107.7
C_{18}-H_{42}	1.0949	0.970	C_{14}-C_{19}-C_{20}	115.1972	118.6
C_{18}-H_{43}	1.0957	0.930	C_{14}-C_{19}-H_{45}	109.2867	109.5
C_{18}-H_{44}	1.0958	0.970	C_{14}-C_{19}-H_{46}	107.9856	-
C_{18}-H_{44}	1.0958	0.930	C_{20}-C_{19}-H_{45}	109.7676	-
C_{19}-H_{45}	1.0995	0.960	C_{20}-C_{19}-H_{46}	108.5682	-
C_{19}-H_{46}	1.0963	0.960	H_{45}-C_{19}-H_{46}	105.5834	109.5
C_{20}-H_{47}	1.0945	-	C_{19}-C_{20}-H_{47}	110.7152	-
C_{20}-H_{48}	1.0955	-	C_{19}-C_{20}-H_{48}	110.9989	-
C_{20}-H_{49}	1.0951	-	C_{19}-C_{20}-H_{49}	112.6839	-
C_{21}- C_{22}	1.5318	1.498	H_{47}-C_{20}-H_{48}	107.6458	107.4
C_{21}-H_{50}	1.0936	-	H_{47}-C_{20}-H_{49}	107.0256	109.5

(*Contd.*)

Table 1 — Structural parameter of the 4B2EH (*Contd.*)

Bond Length (Å)	B3LYP/6–311G (d, p)	Experimental* [12]	Bond Angle (◦)	B3LYP/6–311G (d, p)	Experimental* [13]
C_{21}-H_{51}	1.0954	-	H_{48}-C_{20}-H_{49}	107.5392	-
C_{22}-C_{23}	1.5478	1.489	O_{12}-C_{21}-C_{22}	109.7942	-
C_{22}-C_{27}	1.547	1.412	O_{12}-C_{21}-H_{50}	107.6962	106.1
C_{22}-H_{52}	1.0996	-	O_{12}-C_{21}-H_{51}	110.171	107.14
C_{23}-C_{24}	1.5368	1.435	C_{22}-C_{21}-H_{50}	110.6114	110.21
C_{23}-H_{53}	1.1005	-	C_{22}-C_{21}-H_{51}	110.2073	-
C_{23}-H_{54}	1.0986	-	H_{50}-C_{21}-H_{51}	108.3153	108.2
C_{24}-C_{25}	1.534	1.469	C_{21}-C_{22}-C_{23}	112.8264	113.4
C_{24}-H_{55}	1.0998	-	C_{21}-C_{22}-C_{27}	109.6229	-
C_{24}-H_{56}	1.0941	-	C_{21}-C_{22}-H_{52}	107.3677	-
C_{25}-C_{26}	1.5316	1.509	C_{23}-C_{22}-C_{27}	110.5295	-
C_{25}- H_{57}	1.0989	0.930	C_{23}-C_{22}-H_{52}	108.523	-
C_{25}- H_{58}	1.0992	1.070	C_{27}-C_{22}-H_{52}	107.7913	-
C_{26}- H_{59}	1.0951	-	C_{22}-C_{23}-C_{24}	116.1398	120.2
C_{26}- H_{60}	1.096	-	C_{22}-C_{23}-H_{53}	109.1513	-
C_{26}- H_{61}	1.0954	-	C_{22}-C_{23}-H_{54}	108.0113	-
C_{27} - C_{28}	1.534	1.513	C_{24}-C_{23}-H_{53}	109.644	-
C_{27} -H_{62}	1.0993	1.070	C_{24}-C_{23}-H_{54}	107.9739	-
C_{27}- H_{63}	1.0963	1.070	H_{53}-C_{23}-H_{54}	105.3637	-
C_{28}- H_{64}	1.0945	1.070	C_{23}-C_{24}-C_{25}	112.6065	115.7
C_{28}- H_{65}	1.096	1.060	C_{23}-C_{24}-H_{55}	108.7777	-
C_{28}- H_{66}	1.0946	1.060	C_{23}-C_{24}-H_{56}	110.5164	-
C_{30}- H_{50}	2.3135	-	C_{25}-C_{24}-H_{55}	109.0835	-
Bond Angle (◦)	B3LYP/6–311G (d, p)	Experimental* [13]			
C_2-C_1-C_6	119.3818	119.3	C_{25}-C_{24}-H_{56}	109.4881	-
C_2- C_1-C_7	117.8767	118.9	H_{55}-C_{24}-H_{56}	106.1502	107.9
C_6-C_1-C_7	122.5479	121.2	C_{24}-C_{25}-C_{26}	113.0668	117.0
C_1-C_2-C_3	120.3712	119.9	C_{24}-C_{25}-H_{57}	109.1886	108.8
C_1-C_2-H_{29}	118.8986	120.1	C_{24}-C_{25}-H_{58}	109.532	108.8
C_3-C_2-H_{29}	120.7296	120.4	C_{26}-C_{25}-H_{57}	109.3059	108.8
C_2-C_3-C_4	120.245	121.5	C_{26}-C_{25}-H_{58}	109.5438	108.8
C_2-C_3-H_{30}	119.6436	118.6	H_{57}-C_{25}-H_{58}	105.9556	107.9
C_4-C_3-H_{30}	120.1044	121.1	C_{25}-C_{26}-H_{59}	111.4805	109.7
C_3-C_4-C_5	119.3681	117.8	C_{25}-C_{26}-H_{60}	111.1925	109.7
C_3-C_4-C_{10}	122.8004	123.41	C_{25}-C_{26}-H_{61}	111.0575	109.7
C_5-C_4-C_{10}	117.6678	117.34	H_{59}-C_{26}-H_{60}	107.6318	109.5
C_4-C_5-C_6	120.3811	119.46	H_{59}-C_{26}-H_{61}	107.7982	109.5
C_4-C_5-H_{31}	118.8266	119.5	H_{60}-C_{26}-H_{61}	107.4956	109.5
C_6-C_5-H_{31}	120.7914	119.5	C_{22}-C_{27}-H_{28}	115.9535	-
C_1.C_6-C_5	120.2443	120.4	C_{22}-C_{27}-H_{62}	109.2004	108.8
C_1.C_6-H_{32}	120.0646	119.8	C_{22}-C_{27}-H_{63}	107.2939	108.8
C_5-C_6-H_{32}	119.6829	119.8	C_{28}-C_{27}-H_{62}	109.6554	108.8
C_1-C_7-O_8	121.3936	119.7	C_{28}-C_{27}-H_{63}	108.5293	108.8
C_1-C_7-O_9	119.1654	119.7	H_{62}-C_{27}-H_{63}	105.6954	107.7

(*Contd.*)

Table 1 — Structural parameter of the 4B2EH (*Contd.*)

Bond Length (Å)	B3LYP/6–311G (d, p)	Experimental* [12]	Bond Angle (◦)	B3LYP/6–311G (d, p)	Experimental* [13]
O_8-C_7-O_9	119.3852	121.2	C_{27}-C_{28}-H_{64}	110.5315	109.5
C_7-O_9-C_{13}	122.7342	118.16	C_{27}-C_{28}-H_{65}	111.1694	109.5
C_4-C_{10}-O_{11}	121.4364	124.2	C_{27}-C_{28}-H_{66}	112.7228	109.5
C_4-C_{10}-O_{12}	119.3262	119.7	H_{64}-C_{28}-H_{65}	107.5393	107.7
O_{11}-C_{10}-O_{12}	119.1842	121.3	H_{64}-C_{28}-H_{66}	106.9595	107.7
C_{10}-O_{12}-H_{21}	123.098	124.9	H_{65}-C_{28}-H_{66}	107.6784	107.7
C_9-C_{13}-C_{14}	109.6773	109.9	C_3-H_{30}-H_{50}	120.2652	120.7
C_9-C_{13}-H_{33}	109.3012	109.7	C_{21}-H_{50}-H_{30}	101.4656	-
C_9-C_{13}-H_{34}	108.8234	108.8			

and single bonded at the orientation part of the compound had a maximum and minimum value at the different combinations of this the CCC, CCO, OCO according to C1-C7-O8 = 121.3936/119.7, C1-C7-O9= 119.1654/119.7, C4-C10-O11 =121.4364/ 124.2, C4-C10-O12=119.3262/119.7, O12-C21-H50 =107.6962/106.1, O12-C21-H51 = 110.171/107.14, O11-C10-12 = 119.1842/121.3. The HCH bond angle of maximum and the minima values of the 4B2EH H64-C28-H65=107.5393/107.7, H64-C28-H66=106.9595/107.7, H65-C28-6 = 107.6784/107.7. The Table 1 explain the theoretical values were well matched to the experimental values of it.

Mullikencharges

Mulliken population analysis was used to report the charges on the atoms for optimum geometry. Atomic charges are used to assess the chemical composition of the substance. It is the most complete and effective approach to population analysis[14]. The Mulliken charge is directly related to the chemical bonds that exist in the molecule since it quantifies the electronic structure's variation under atomic displacement and is instantly connected to the vibrational properties of the molecule. It affects molecular systems' electrical structure, polarizability, dipole moment, and other properties[15]. Charge distributions across the atoms imply that the molecule's charge transfer involves the creation of donor and acceptor pairs. Using the 6-311++G (d, p) basis sets mentioned in (Table 2), B3LYP was utilized to calculate the Mulliken population analysis in the 4B2EH molecule[16]. Its electrophilic character is demonstrated by the oxygen atom's charges of O11 → 0.474 eV, O12 → 0.443 eV, and the positive charges on some carbon atoms, 10→ 0.536 eV, C18 and C26 → 0.309 eV, and C20 and C28 → 0.314 eV. The charges of hydrogen atoms

Table 2 — Mulliken Atomic Charges of 4B2EH

Atoms	Charges (eV)	Atoms	Charges (eV)
C_1	0.053	H_{34}	0.110
C_2	-0.110	H_{35}	0.101
C_3	-0.119	H_{36}	0.095
C_4	0.055	H_{37}	0.087
C_5	-0.088	H_{38}	0.085
C_6	-0.111	H_{39}	0.106
C_7	0.506	H_{40}	0.094
O_8	-0.450	H_{41}	0.087
O_9	-0.425	H_{42}	0.093
C_{10}	0.536	H_{43}	0.096
O_{11}	-0.474	H_{44}	0.102
O_{12}	-0.443	H_{45}	0.093
C_{13}	0.019	H_{46}	0.098
C_{14}	-0.065	H_{47}	0.099
C_{15}	-0.173	H_{48}	0.106
C_{16}	-0.170	H_{49}	0.101
C_{17}	-0.173	H_{50}	0.082
C_{18}	-0.309	H_{51}	0.125
C_{19}	-0.183	H_{52}	0.097
C_{20}	-0.314	H_{53}	0.098
C_{21}	0.011	H_{54}	0.084
C_{22}	-0.064	H_{55}	0.084
C_{23}	-0.175	H_{56}	0.106
C_{24}	-0.170	H_{57}	0.094
C_{25}	-0.172	H_{58}	0.086
C_{26}	-0.309	H_{59}	0.093
C_{27}	-0.182	H_{60}	0.095
C_{28}	-0.314	H_{61}	0.102
H_{29}	0.111	H_{62}	0.084
H_{30}	0.154	H_{63}	0.100
H_{31}	0.131	H_{64}	0.098
H_{32}	0.115	H_{65}	0.109
H_{33}	0.104	H_{66}	0.095

vary from H50 → 0.082 eV to H30 → 0.154 eV. With the maximum charge at H30 → 0.154 eV, the hydrogen atoms show comparatively homogeneous charges, indicating a variety of bonding conditions. The findings show that the oxygen atoms have areas of high electron density, which makes them possible nucleophilic sites, and the highly charged carbon atoms are likely electrophilic sites, which are necessary for binding contacts and reactivity.

HOMO LUMO Analysis

Chemically speaking, boundary molecular orbitals are the lowest unoccupied molecular orbital (LUMO) and the highest occupied molecular orbital (HOMO) of a molecule. These orbitals are essential for figuring out molecular reactivity and other properties related to its uses[17]. 4B2EH 's chemical reactivity descriptors were observed using the B3LYP/6-311++G (d, p) method (Fig. 3). shows crisp views of border molecular orbitals using Gauss View 5.0 software. The numerical derivation of theoretical energy parameters for 4B2EH from Equations 1 to 21 exhibited insights about the upcoming discussed parameters and their values. The Homo-Lumo energy gap is shown to have a sizable energy gap of 4.9348 eV, with Homo-Lumo values of -6.7166 eV and -1.7818 eV. The named compound's stability is indicated by the negative values[18]. The compound's stability is validated by its chemical hardness, which in this investigation is 2.4674 eV. An electrophilicity index maximum range of 3.6588 eV, which indicates biological activity, is confirmed by the observation. The 4B2EH chemical is non-toxic, as indicated by its low softness value of 0.4052 eV^{-1}. The range of 4B2EH in industrial and medicinal applications is determined by its chemical softness[19]. Its electronic stability is further reinforced by its ionization potential of 6.7166 eV and electron affinity of 6.7166 eV. Moderate reactivity is suggested by electronegativity 4.2492 eV and electrophilicity 3.6588 eV, with a greater electron-donating capacity ω− = 6.0918 eV than electron-accepting capacity ω+ = 1.8426 eV. Ionization potential (I), electron affinity (A), chemical potential (μ), electronegativity (χ), chemical hardness (η), electrophilicity index (ω), and global softness (σ) were all calculated using Koopman's theorem[20]. The computed chemical reactivity descriptors are listed in (Table 3). These properties indicate that 4B2EH is a molecule with biological action. The UV-Vis at the gas phase with the 3 states denotes the energy gap values which are similar to the both theoretical and experimental energy gap values as for wavelength concerning the 302nm / 4.1059 eV, 273nm /4.5421 eV, 262 nm / 4.7328 eV, 469/4.617 eV.

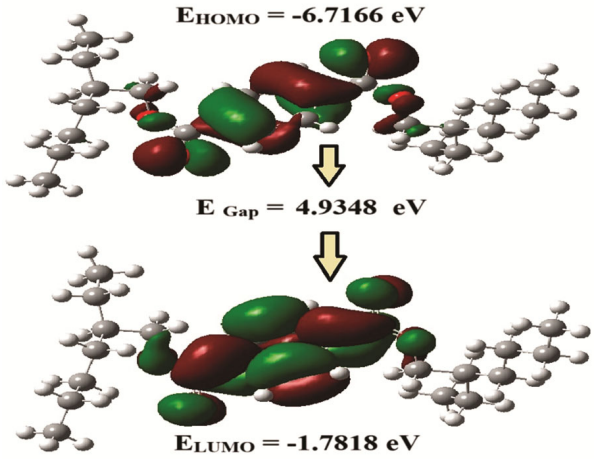

Fig. 3 — E_{Homo}, E_{Lumo}, E_{Gap} of 4B2EH molecules

Numerical derivation of theoretical energy parameters for 4B2EH

E_{HOMO} = -6.7166 eV ... 1

E_{LUMO} = -1.7818 eV ... 2

Energy Gap = E_{LUMO} - E_{HOMO} =4.9348eV ... 3

Ionization Potential (IP) = − E_{HOMO} Substituting Eq. 1

Ionization Potential (IP) = 6.7166 eV

Table 3 - Chemical stability & reactivity on 4B2EH

Electronic Properties	Values eV	Electronic Properties	Values eV
E_{HOMO}	-6.7166 eV	Chemical hardness (η)	2.4674 eV
E_{LUMO}	-1.7818 eV	Chemical softness (σ)	0.4052 eV^{-1}
ΔE	4.9348 eV	Electrophilicity Index (ω)	3.6588 eV
ωIonization potential (IP)	6.7166 eV	Nucleophilicity Index 1/	0.1366 eV^{-1}
Electron affinity (EA)	1.7818 eV	Electron donor power (ω^-)	6.0918 eV
Electronegativity (χ)	4.2492 eV	Electron acceptor power (ω^+)	1.8426 eV
Chemical potential (μ)	-4.2492 eV	ΔNmax (eV)	-1.7221 eV

Electronic Affinity (EA) = $-E_{LUMO}$ Substituting Eq. 2

Electronic Affinity (EA) = 1.7818 eV ... 4

Electronegativity (χ) = $\frac{IP+EA}{2}$ Substituting Eqs. 3 & 4

$= \frac{(-E\ HOMO + (-E\ LUMO))}{2} = \frac{[(6.7166) + (1.7818)]}{2}$

Electronegativity (χ) = 4.2492 eV ... 5

Electronegativity (χ) = − Chemical Potential (μ) ... 6

Chemical Potential (μ) = -4.2492 ... 7

Chemical hardness (η) = $\frac{IP-EA}{2}$ ... 8

$= \frac{(-E\ HOMO+E\ LUMO)}{2}$ Substituting Eq. 3 & 4 $= \frac{6.7166-1.7818}{2}$

Chemical hardness (η) = 2.4674 eV ... 9

Chemical Softness (σ) = $\frac{1}{\eta}$ Substituting Eq. 9 ... 10

Chemical Softness (σ) = 0.4052 eV^{-1} ... 11

Electrophilicity Index (ω) = $\frac{\mu 2}{2\eta} = \frac{(-4.2492)^2}{2\ (2.4674)}$ = 3.6588 ... 12

Electrophilicity Index (ω) = 3.6588 eV ... 13

Nucleophilicity index = $\frac{1}{\omega}$ Substituting Eq. 13 = $\frac{1}{(3.6588)}$ ... 14

Nucleophilicity N index = 0.1366 eV^{-1} ... 15

Electron Acceptor Power (ω^+) = $\frac{(IP+3EA)^2}{16\ (IP-EA)}$ Substituting Eq. 3 & 4 ... 16

Electron Acceptor Power (ω^+) = 1.8426 eV ... 17

Electron Donor Power (ω^-) = $\frac{(3IP+EA)^2}{16\ (IP-EA)}$ Substituting Eq. 3 & 4 ... 18

Electron Donor Power (ω^-) = 6.0918 eV ... 19

Additional Electronic Charge

$\Delta N\ max = \frac{\mu}{\eta}$ eV Substituting Eq. 7 & 9 $\Delta N\ max$ = -1.7221 eV ... 20

Additional Electronic Charge ($\Delta N\ max$) = -1.7221 eV ... 21

FT-IR and vibrational assignment

The FT-IR spectra of 4B2EH (Fig. 4) show the most important vibrations, including CH, CC, OC, CCO, HCCC, HCC, HCH, and HCCO, HCO, HCOC, CCCC, CCC, OCO, OCOC, OCCC. The experimental and computational FT-IR wave numbers are tabulated in the table. The PED findings are in agreement with the IR absorption intensities of 4B2EH as displayed in the tables. Strong tools for analyzing and allocating vibrational modes in molecular systems, interpreting vibrational spectra, applying frequency scaling, and assisting in the validation of computational techniques against experimental data are Gauss View 6.0 and VEDA 04 software. The DFT-B3LYP functional with 6-311++G (d, p) basis sets in the gas phase is used to carry out the vibrational computations which is shown in (Fig. 4, and Table 4) [21].

Although the benzene ring is symmetric, rotational axes and mirror planes are broken by the large 2-ethylhexyl chains. The molecule is therefore given the C1 symmetry group. 1, 4-Benzenedicarboxylic Acid, Bis (2-Ethylhexyl) Ester is a non-linear molecule due to its benzene core and the flexibility of its 2-ethylhexyl chains. The straight geometry necessary for linearity is absent. Vibrational Modes may be calculated for these non-linear features of the

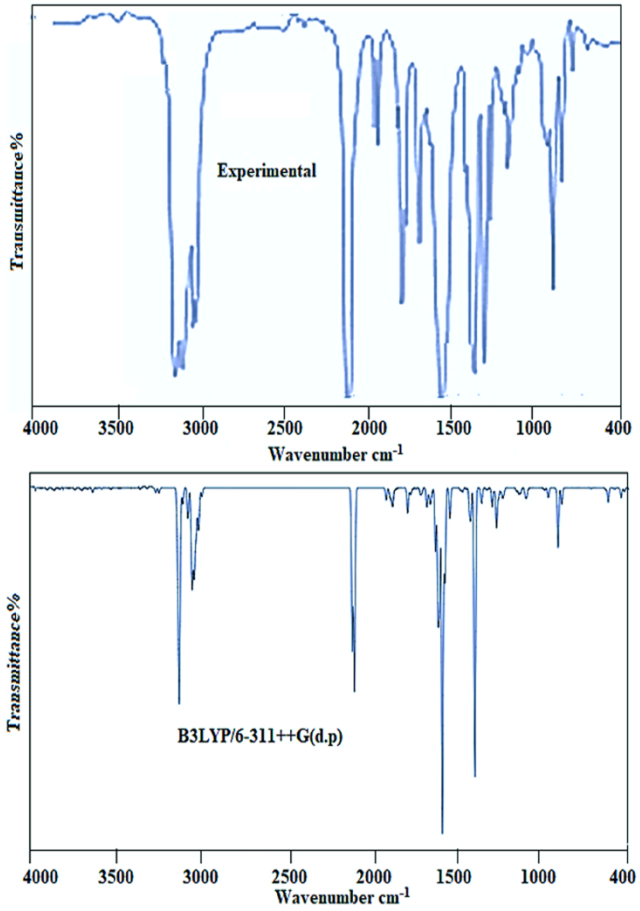

Fig.4 — FT-IR and vibrational assignment 4B2EH

Table 4 — FT-IR and Vibrational Assignment 4B2EH

B3LYP	Experimental	Vibrational assignment	PED	B3LYP	Experimental	Vibrational assignment	PED
3223	3221	υCH	99	1518	-	δHCC	65
3222	3222	υCH	46	1517	-	δHCC	25
3208	-	υCH	42	1514	1514	τHCCC+δHCC	13+39
3207	-	υCH	24	1513	-	δHCC	100
3120	-	υCH	68	1512	-	δHCC	40
3118	-	υCH	33	1506	-	δHCC	48
3115	-	υCH	26	1505	-	δHCC	51
3114	-	υCH	64	1503	-	δHCC	69
3111	-	υCH	71	1499	-	δHCC	71
3110	-	υCH	85	1496	-	δHCC	70
3109	3104	υCH	46	1491	-	δHCC	79
3105	-	υCH	70	1443	-	υCC	16
3094	3094	υCH	51	1435	-	τHCOC	14
3070	-	υCH	55	1433	-	δHCC	74
3069	3069	υCH	56	1431	-	τHCOC	13
3054	-	υCH	93	1430	-	δHCC	53
3050	-	υCH	47	1427	-	δHCC	50
3048	3048	υCH	28	1426	-	δHCC	43
3044	-	υCH	96	1417	-	τHCCC	-13
3043	-	υCH	36	1416	-	τHCCC	32
3042	-	υCH	92	1403	1408	τHCCC	-27
3041	-	υCH	70	1402	-	τHCCC	53
3039	-	υCH	62	1383	1384	τHCCC	28
3038	3038	υCH	98	1382	1381	τHCCC	13
3036	-	υCH	38	1376	1378	δHCC	20
3030	-	υCH	56	1375	-	τHCCC+δHCC	12+20
3022	-	υCH	39	1352	1356	υCC	31
3021	-	υCH	97	1345	-	δHCC + δHCO	23+45
3018	-	υCH	100	1344	1340	δHCC+ δHCO	42+12
3014	3012	υCH	91	1339	-	δHCC	29
3005	3009	υCH	89	1336	-	δHCC+ δHCO	18+12
3002	3001	υCH	94	1333	-	δHCC	35
1815	-	υOC	90	1329	-	τHCCC+ δHCC	11+36
1804	1801	υOC	90	1327	-	δHCC	17
1664	1668	υCC	28	1314	-	δHCC	29
1615	-	υCC	31	1311	1310	δHCC + δHCO	10+20
1544	-	δHCC	33	1299	1288	υCC	24
1529	-	δHCC	49	1292	1295	τHCCC	11
1526	-	δHCC	33	1271	1276	δHCC	28
1523	-	τHCCC + δHCC	25+57	1266	-	δHCC	33
1520	-	δHCC	52	1244	-	τHCCC + δHCC	10 + 4
1243	1250	δHCC	63	641	-	δCCC	38
1208	1203	δHCC	38	576	-	δOCC	25
1183	-	δHCC	11	570	-	δOCC	22
1170	1174	τHCCC + υCC	14+23	506	-	δCCC	41
1144	1141	δHCC + υCC	17+20	504	-	δCCC	33
1127	-	υOC + υCC	36+12	495	-	υCC	12
1124	-	υOC + υCC	46+27	471	-	δCCC	12
1096	1094	τHCCC + υCC+ υOC	10+ 40+16	462	-	δCCC	27
1072	-	υCC	30	422	-	τHCCC+ τCCCC	34
1068	-	υCC	48	400	-	δCCC + γCCCC	10+10

(*Contd.*)

Table 4 — FT-IR and Vibrational Assignment 4B2EH

B3LYP	Experimental	Vibrational assignment	PED	B3LYP	Experimental	Vibrational assignment	PED
1063	-	υCC	14	354	-	δCCO+ δCCC + γCCCC	18+46 +12
1055	1054	τHCCC + υCC	10+11	326	-	δCCC	29
1052	-	υCC	32	300	-	δCCC + υCC	12+10
1049	1047	υCC	38	265	-	δCOC	19
1043	1046	δCCC + υOC	19+13	259	-	δCCC	20
1032	1037	υOC	30	249	-	τHCCC	71
1022	1025	δCCC + υCC + δCCC	11+17 +22	246	-	τHCCC	31
1015	1013	υCC	29	236	-	τHCCC	50
1012	-	υCC	18	233	-	τHCCC + δCOC	13+15
987	989	τHCCC + γCCCC	27+30	215	-	δCCC	11
994	995	υOC	10	212	-	δCCO + δCCC	10+24
919	-	τHCCC	10	201	-	δCCO + γCCCC	20+15
917	-	τHCCC	11	170	-	δCOC + δCCC	18+21
910	911	υCC	23	146	-	τCCCC	20
907	904	τHCOC + υCC	16+21	137	-	τCCCC	58
880	885	τHCCC + υCC	11+28	104	-	τCCCC	12
866	869	τHCCC	47	97	-	τOCCC + τCCCC	10+14
806	805	γOCOC	10	91	-	τCCCC	15
802	801	δCCC + υCC	18+12	78	-	τCCCC	39
795	-	τHCCC	21	77	-	τCOCC	13
791	-	τHCCC	27	70	72	τCCCC	41
778	-	τHCCC	22	68	-	τCCCC	52
776	770	τHCCC	15	50	-	τCCCC	95
740	-	τHCCC + δHCC	42+11	46	-	τCCCC	26
737	736	τHCCC + δHCC	44+12	32	-	τCCCO+ τCCOC	28+14
732	731	γOCOC	54	21	-	τCOCC	30
714	-	δOCO	11	14	-	τCCOC+ τCCCO	43+17
705	701	τCCCC + γOCOC	42+10	12	-	τCCOC+ τOCCC	41+21
653	650	δOCO	39	8	-	τCCCO+ τCCOC	54+19

chemical using the 3N−6 by C24H38O4. Six out of simple bending modes, sixty-five stretching modes, sixty-four bending modes, and fifty-seven torsional modes yield the 192 vibration modes. Experimental and theoretical wave numbers are compared through normal mode vibrational experiments. Aliphatic Chains' C–H Stretching ~2800–3000 cm^{-1}, the C-H bonds in the 2-ethylhexyl chains and the C-H Bending Methyl and Methylene Groups at the ~1350–1470 cm^{-1} stretch both symmetrically and asymmetrically. Bending vibrations of C-H bonds connected to the benzene ring cause out-of-plane C-H bending in the aromatic ring at around 650–900 cm^{-1}. The hetero aromatic structure in the gas phase shows the existence of C–H stretching vibration in the area between 3100 and 3300 cm^{-1}, which is unique for the rapid detection of C–H stretching vibration[22]. At 99%, 46%, 28%, 98%, 91%, 89%, and 94% PED values, the CH symmetric stretching of 3223/3221 cm^{-1}, 3222/3222 cm^{-1}, 3048/3048 cm^{-1}, 3038/3038 cm^{-1}, 3014/3012 cm^{-1}, 3005/3009 cm^{-1}, and 3002/3001 cm^{-1} corresponds to the theoretical and experimental values. With 13%, 39%, and 11% PED, the twisting and scissoring bending vibration at HCCC & HCC is represented by wave numbers 1514/1514 cm^{-1} and 1292/1295 cm^{-1}. Wagging bending and PED values at the HCCC were 28% at the 1383/1384 cm^{-1}, 13% at the 1382/1381 cm^{-1}, and 15% at the 776/770 cm^{-1}. With 13%, 39%, and 11% PED, the twisting and scissoring bending vibration at HCCC & HCC is represented by wave numbers 1514/1514 cm^{-1} and 1292/1295 cm^{-1}. Along with wagging bending, the PED values at HCCC were 28% at 1383/1384 cm^{-1}, 13% at 1382/1381, 15% at 776/770 cm^{-1}, and 44% at 737/736 cm^{-1}[23]. HCC wagging at 1344/1340 was 42%, HCC rock at 1311/1310 was 20%, HCC scissoring at 1271/1276 was 28%, and HCC 737/736 was 12%. Similarly, the ester carbonyl groups

(−C=O-C=O−C=O) stretched symmetrically and asymmetrically with unsaturated C=O stretching at the carbonyl group, ranging from ~1700 to 1750 cm^{-1}. The stretching vibrations of the C–O bonds in the ester groups were around 1000–1300 cm^{-1} in a saturated C–O stretching in the ester linkage. 70/72 twisting CCCC with 41% PED, and 1352/1356 rocking CC with 31%. 1341/1340 cm^{-1} rock mode of vibration with HCO 20%, 1344/1340 cm^{-1} wagging vibration HCO with 12%. The compound's aromatic C=C stretching occurs in vibrational modes of the benzene ring at around 1450–1600 cm^{-1}, whereas C stretching and bending occurs at approximately 800–1100 cm^{-1}, [24]. The PED values with vibrational assignment according to the orientation and position of the carboxylic group and the Ethylhexyl of the compound are shown by the stretching and bending of the carbon-carbon bonds in the aliphatic chains and benzene ring as per the litterateur study, in addition to the theoretical and experimental investigations. 653/650 cm^{-1} scissoring mode of vibration is done at the OCO bending with 39% PED, 705/701 cm^{-1} Twisting CCCC with PED 42, and wagging of out of the plain OCOC may be done with PED 10%. 54% PED with 732/731 cm^{-1} wagging with out-of-plane OCOC.

Druglikness

This prediction informs users about the medicine's effectiveness and whether or not the ligand under investigation possesses characteristics that are typical of an orally active agent. This prediction is based on a previously developed hypothesis by Lipinski et al., called Lipinski's rule of five[25]. The chemical structures of the medications were converted into their standard simplified molecular input line entry system (SMILE) and then entered into the SwissADME computer to estimate *in silico* pharmacokinetic parameters. A compound's total polar surface area, number of hydrogen donors, hydrogen acceptors, and rotatable bonds are all provided by the SwissADME predictor shown in (Table 5).

Furthermore, the ligands were subjected to Lipinski screening with SwissADME and Pre-ADMET predictors. The organ toxicities and toxicological endpoints of the ligands. According to Lipinski's rule, potential compounds should have the following physicochemical properties: A molecular mass below 500 Da, (i) fewer than five hydrogen bond donors (HBDs), (ii) fewer than ten hydrogen bond acceptors (HBAs), (iv) log P not more than five, and (v) total polar surface area (TPSA) not more than 140A is all requirements. Based on the SwissADME computed data, all of the synthesized compounds in this study have zero breaches of Lipinski's rule of five[26]. Chemicals may therefore be appropriate for studies on their antibacterial, antioxidant, and anticancer qualities. It may become more drug-like and effective if its structure is altered by adding polar groups or shortening the chain.

MEP Analysis

The preferred position of the electrophile and nucleophile in terms of the molecule's electrostatic potential is made clear by employing color grading. MEP is used to analyze the reactive locations and dynamic binding site of the title chemical with the color areas shown in (Fig. 5) [27]. The net electrostatic effect which is produced for the molecule's charge distribution is also produced by it. Moreover, it uses color grading on the molecule surface to offer molecular size, shape, and neutral, positive, and negative charges. This study provides specifics on the drugs' physiochemical properties[28]. Since we are aware that the potential between adjacent atoms determines their interactions, the electrostatic potential [V (r)] can be used to quantify these interactions[29].

Table 5 — Lipinski's values of 4B2EH

Descriptor	Value
Molecular Weight	390.564
LogP	6.433
Acceptors	4
Donors	0
Surface Area	170.550

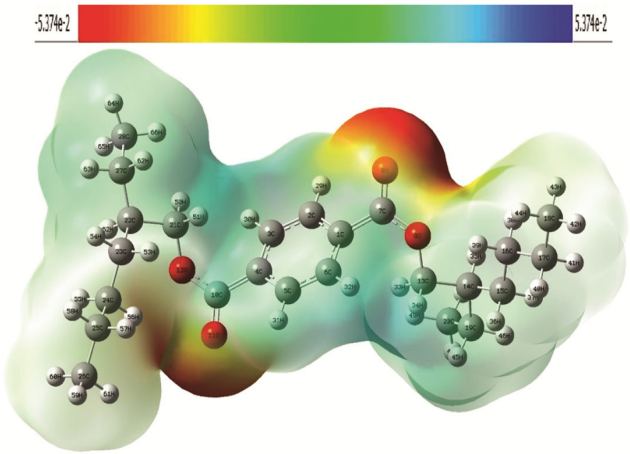

Fig.5 — MEP of 4B2EH

$$V(r) = \sum \frac{Z_R}{R_A - r} - \int \frac{\rho\,(r')}{(r' - r)}$$

The optimized shape of the title molecule is used to create the MEP map, which is seen in (Fig. 5). On the MEP map, blue indicates areas with low electron density and red indicates places with high electron density. This displays the molecule surface's electrostatic potential distribution. Atoms of hydrogen bonded to aromatic carbons have the lowest electron density, whereas oxygen atoms have the highest. To forecast possible reaction locations, this information is helpful. In this 4B2EH the Oxygen grouped to a carbon acts as a carboxylic group which is indicated as red representing the high electron density thatleads to nucleophilicity. The potential value starts from the -5.374e^{-2} to 5.374 e^{-2}.

NBO Analysis

NBO analysis is a useful technique for determining intramolecular and intermolecular bonding interactions and offers a good foundation for studying charge transfer in molecular structure[30]. By examining various second-order interactions between the filled orbitals of one subsystem and the vacant orbitals of another subsystem, the NBO computation calculates the intermolecular delocalization or hyperconjugation. The interaction results in a loss of occupancy from the localized NBO of the idealized Lewis structure into an empty non-Lewis orbital. The stabilization energy E (2) related to electron delocalization between the donor and acceptor is calculated as follows for each donor NBO (i) and acceptor NBO (j):

$$\mathrm{E}\,(2) = \Delta E_{ij} = q_i \frac{F^2_{(i,j)}}{\varepsilon_j - \varepsilon_i}$$

The E (2) value increases with the strength of the interaction between electron donors and electron acceptors. Here, qi is the donor-orbital occupancy, F (i, j) is the Fock matrix element between the natural bonding orbitals, and ε_i and ε_j are the orbital energies of diagonal elements[31, 32]. To shed light on the electron density delocalization inside the molecule, the title molecule was subjected to NBO analysis at the B3LYP/6–311++G (d, p) level. Details of the important interactions are shown in (Table 6). Lone pair (LP) contributions like O_8 (LP2) → $C_7 – O_9$ (σ*) and O_{11} (LP2) → $C_{10} – O_{12}$ (σ*) are noteworthy interactions in the examined molecule. Their stabilization energies are 32.07 kcal/mol and 33.03 kcal/mol, respectively. Strong delocalization effects are highlighted by one of the strongest interactions, $C_4 – C_5$ (π*) → $C_{10} – O_{11}$ (π*), which exhibits E (2) =183.43 kcal/mol. Other π → π* interactions, such as $C_4 – C_5$ (π) → $C_{10} – O_{11}$ (π*), show a high stabilization energy of 24.26 kcal/mol. Meanwhile, LP → π* and σ → σ* interactions have a major role in the stability of the system. These results highlight a complex network of delocalized electrons and donor-acceptor interactions that greatly improve molecule stability. The findings of the NBO analysis

Table 6 — Donor and Acceptor interaction NBOs analysis on 4B2EH molecules

Donor (i)	Type	Acceptor (j)	Type	E (2) (Kcal/ mol-1)	E (j) -E (i) (a. u.)	F (i, j) (a. u.)
O11	LP (2)	C4 - C10	σ*	14.99	0.84	0.102
O8	LP (2)	C1 - C7	σ*	15.29	0.84	0.104
C1 - C6	π*	C7 - O8	π*	17.28	0.01	0.024
C2 - C3	π	C4 - C5	π*	17.98	0.29	0.065
C4 - C5	π	C1 - C6	π*	18.23	0.28	0.064
C1 - C6	π	C2 - C3	π*	18.61	0.28	0.065
C21 - H50	π	C 3 - H30	σ*	21.16	1.05	0.134
C2 - C3	π	C1 - C6	π*	22.02	0.29	0.072
C4 - C5	π	C2 - C3	π*	22.16	0.28	0.071
C1 - C6	π	C4 - C5	π*	22.64	0.29	0.072
C 4 - C5	π	C10 - O11	π*	24.26	0.3	0.078
O8	LP (2)	C7 - O9	σ*	32.07	0.64	0.13
O11	LP (2)	C10 - O12	σ*	33.03	0.64	0.132
C3 - H30	σ	C21 - H50	σ*	44.65	1.06	0.195
O12	LP (2)	C10 - O11	π*	45.27	0.36	0.115
O9	LP (2)	C7 - O8	π*	46.58	0.36	0.115
C4 - C5	π*	C10 - O11	π*	183.43	0.01	0.078

open up opportunities for more research in fields like material science, catalysis, and biological activity by offering insightful information on the molecule's electrical structure and reactivity.

Topological Analysis

A complete understanding of electron distribution and bonding is provided by the Electron Localization Function (ELF) and Localized Orbital Locator (LOL), which are frequently employed for surface and topological investigations of molecular systems. ELF τ (r) and LOL$_{\tau}$(r), which explain electron localization in terms of density and orbital interactions, are the foundation of these techniques, which help interpret covalent bonds and electronic structures[33, 34]. Using Multiwfn 3.7 software, ELF and LOL analyses were performed on the 4B2EH in this study. The results are displayed in (Figs. 6 & 7) as colour field projection maps and contour maps. The blue-to-red colour gradient represents the ELF values, which range from 0.0 to 1.0. Aside from the regions that surround atomic nuclei, red areas denote regions with high electron localization at C7, O8, O9 of the carboxylic group, like lone pairs, whereas blue regions that join atoms show lesser electron localization, which is typical of covalent bonds. This is enhanced by the

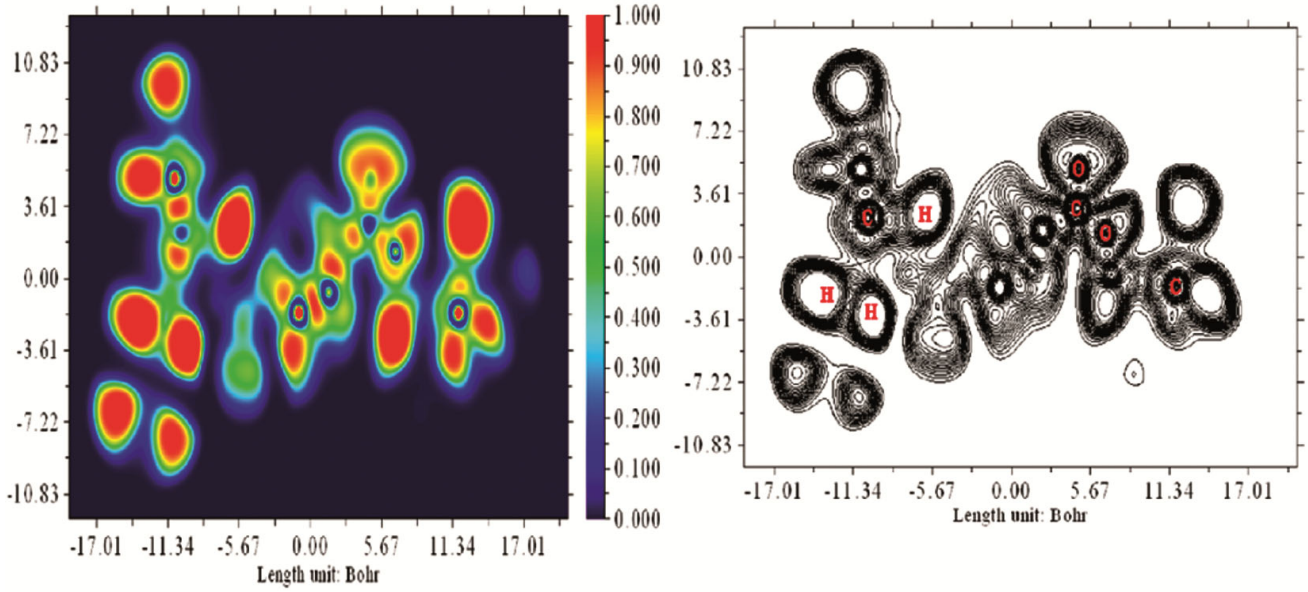

Fig. 6 — ELF map of 4B2EH

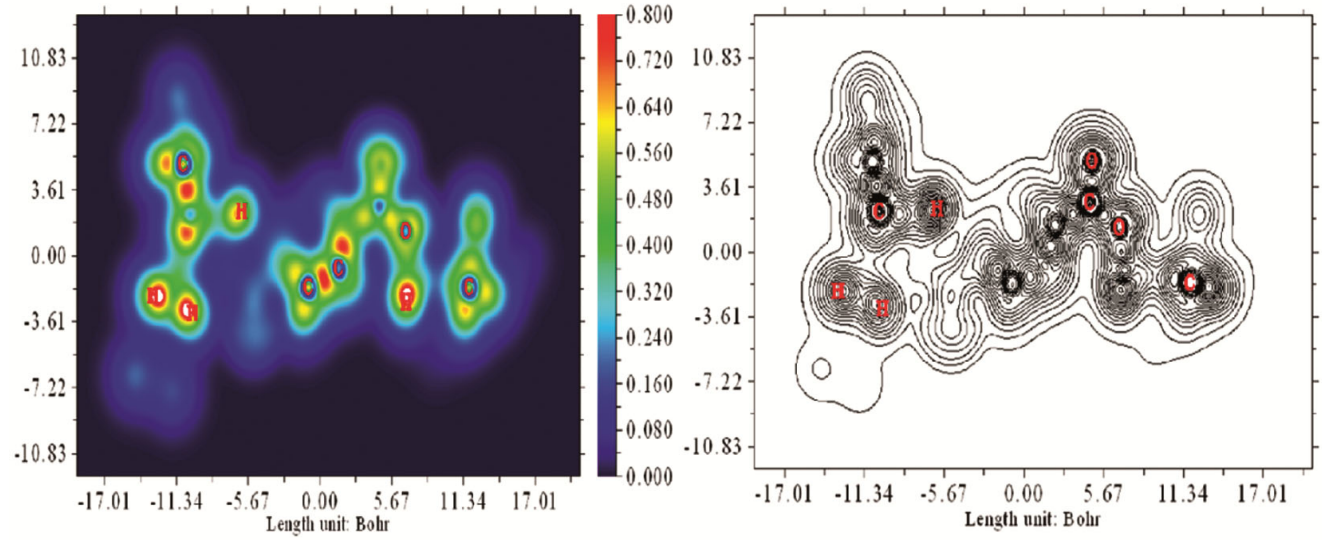

Fig. 7 — LOL map of 4B2EH

LOL analysis, which offers further information for values between -17.01 and 17.01 Bohr. Electron localization is shown by the matching colour scale, which ranges from blue to red 0.0 to 0.80[35].Whereas blue regions, which frequently have wider contour spacing, indicate areas of poorer electron localization, red portions in LOL maps indicate electron-rich places, such as lone pairs and bonding regions. In addition to disclosing the molecule's electrical structure, these investigations offer important insights into the system's atomic connections and biological interactions. Combining ELF and LOL research improves knowledge of bonding properties and electron density distribution, which makes it a crucial method for molecular research[36].

Reduced density gradient of 4B2EH

To investigate the various types of non-covalent interactions between molecules and as a crucial instrument for comprehending research on chemical reactivity. RDG analysis is a visual method that makes 3TMH and covalent interactions more complex[37]. Figures 8 and 9 show the colour-filled RDG map and scatter map of the 4B2EH compound

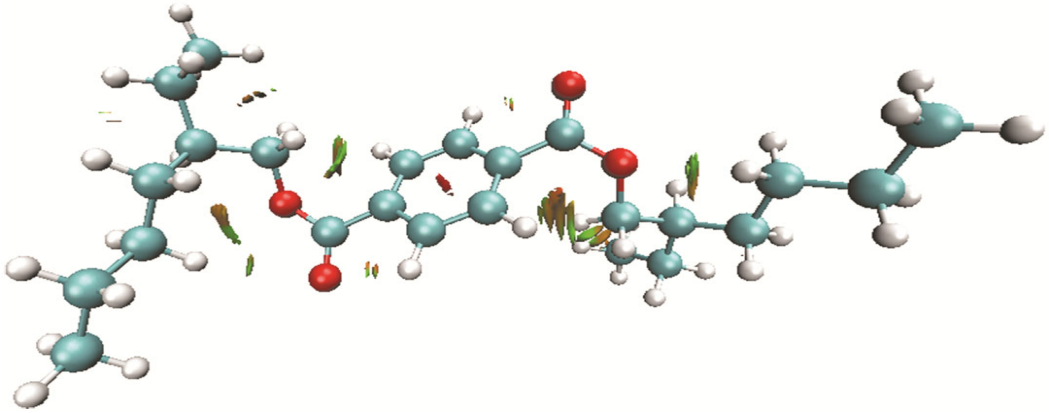

Fig. 8 — Van der Waals, Steric effect with Hydrogen bonding of 4B2EH

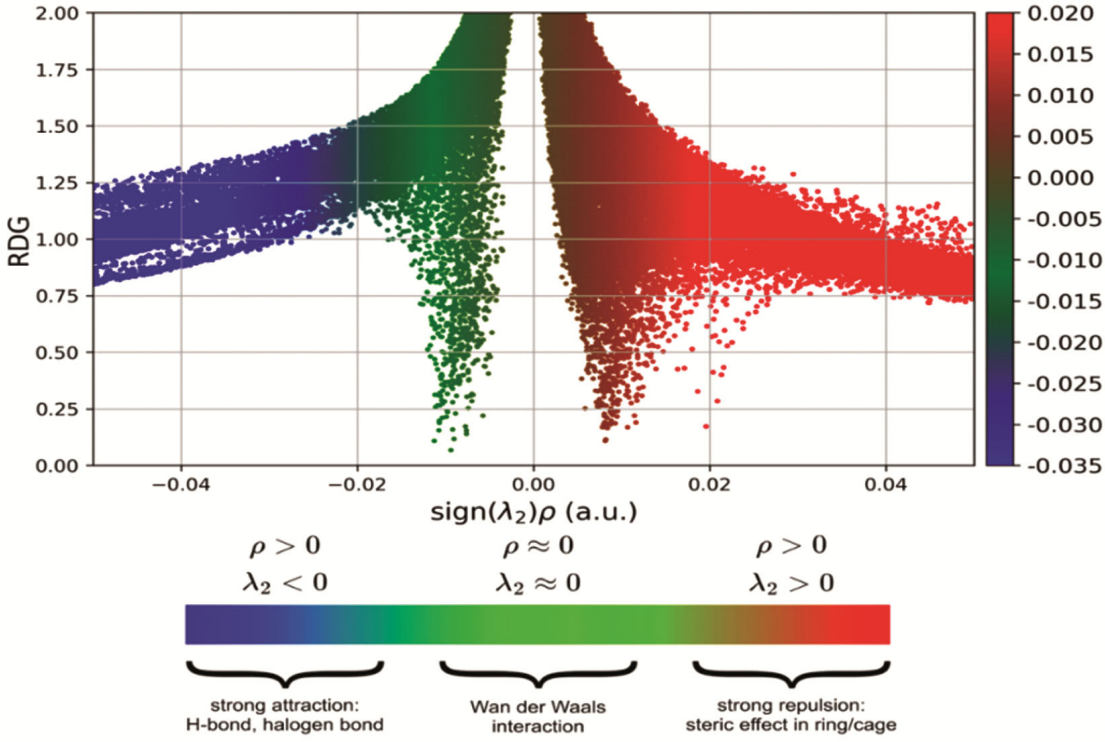

Fig. 9 — Sign (λ_2) ρ plot of 4B2EH

RDG, which were produced using the software analyser VMD 1.9.2 and Multiwfn 3.7. The characteristics of electron density serve as the foundation for the interactions[38]. On the other hand, hydrogen interactions show large negative values of λ2 with high-density values (ρ> 0, λ2 < 0) ; van der Waals interactions, on the other hand, show values of λ2 and density that are nearly equal to zero (ρ≈0, λ2 ≈0) ; and strong repulsive interactions are found in regions where λ2 is significantly positive and density values are high (ρ> 0, λ2 > 0) [39]. The electronic density (ρ) and its gradient (∇ρ) are the sources of the dimensionless scalar quantity known as the Reduced Density Gradient:

$$RDG = \frac{1}{2\,(3\pi^2)^{\frac{1}{3}}} \frac{|\nabla\rho|}{\rho 4/3}$$

ρ: Electron density at a location in space, and |∇ρ|: Electron density gradient magnitude. The van der Walls contact is the primary interaction in this molecule, and the red color indicates the steric repulsion between the half-ring structure and the benzene ring center. A significant steric impact is often seen in organic unit atoms when the repulsive contact (red zone) is seen.The region with a positive sign (λ2) ρ in (Fig. 9) spans from 0.035 to 0.020 a.u. Interactions between the hydrogen atoms in the organic group are observed through the van der Waals effect (the green zone) [40]. Another van der Waals contact exists between the molecule's organic and inorganic groups. The sign region of (λ2) ρ = 0 is where the van der Waals interactions take place in (Fig. 9). Additionally, Figure 9 has dark blue specks. This strong attractive interaction is situated between -0.05 and -0.02 a.u. and has a negative sign (λ2) ρ[41]. In addition to the steric effects between C_1=C_2-C_3=C_4-C_5=C_6, O_{11}---H_{31}, and O_8---H_{29} [42], this graph displays the van der Waals forces between the molecules C_{10}-O_8-O_9-C_{13}-H_{36}-H_{37} and C_{10}-O_{11}-O_{12}-C_{21}-H_{50}-H_{51}. There exist hydrogen bonding sites in 4B2EH since the results of this research are in good agreement with the docking studies. When predicting the likelihood of a molecule docking with a receptor based on its capacity to dock ligands, the effects are crucial in DFT investigations.

UV–Vis, TD-DFT, DOS analysis of 4B2EH

The Shimadzu UV-Vi spectrometer was used to measure the UV-Vi's. A simple and direct method for figuring out the band gap energy of organic p-conjugated systems is UV-Vis[41]. The following equation can be used to determine the optical band gap: Eg = 1242/ λth, where λth is the threshold wavelength (in nm), determined from the beginning of the absorption spectrum, and Eg is the optical energy band gap (in eV). Based on the DFT/B3LYP/6-311++G (d, p) method, which was calculated in the gas phase and correlated with experimental UV-Visible spectra, quantum chemical theory was used to interpret the electronic transition features of 4B2EH, which were discovered through the UV-Visible spectra and related properties of oscillation strengths (f), excitation energy (eV), and absorption band (nm). We analyze the compound of antibonding, bonding, and nonbonding characteristics in this manner. We have used time-dependent density functional theory (TDDFT) on the optimized structure in gas to examine the UV spectra[42]. All of these characteristics experience significant HOMO-LUMO orbital changes upon absorption of UV radiation. The n-p transition is less noticeable than the p-p transition. The n or p orbitals shift to an excited state in the absorption spectroscopy approach. Additionally, after reporting the molecular orbitals' energy, we computed the energy gap between the major peaks of the spectra's molecular orbitals and the border HOMO–LUMO orbitals[43]. The UV spectrum in the gas phase is depicted in (Fig. 10) and the molecule's computed wavelength, energy, bond gap, and oscillator strength are shown in (Table 7).

Table 7 — TDDFT for the 4B2EH

Solvent Gas	Oscillation Strength f	Energy cm-1	Max (nm)	Bandgap eV	Major Contribution energy	Minor Contribution energy
S1	0.0361	33060	302.47	4.0990	H-2->LUMO (19%), HOMO->LUMO (69%)	H-5->LUMO (2%), H-1->LUMO (3%)
S2	0.0019	36609	273.15	4.5390	H-2->LUMO (33%), H-1->LUMO (41%),	HOMO->L+1 (18%) HOMO->LUMO (3%)
S3	0.0503	38141	262.18	4.7290	H-2->LUMO (37%), HOMO->LUMO (15%), HOMO->L+1 (22%)	H-1->LUMO (11%) H-3->LUMO (6%)
	Experimental		269 (nm)			

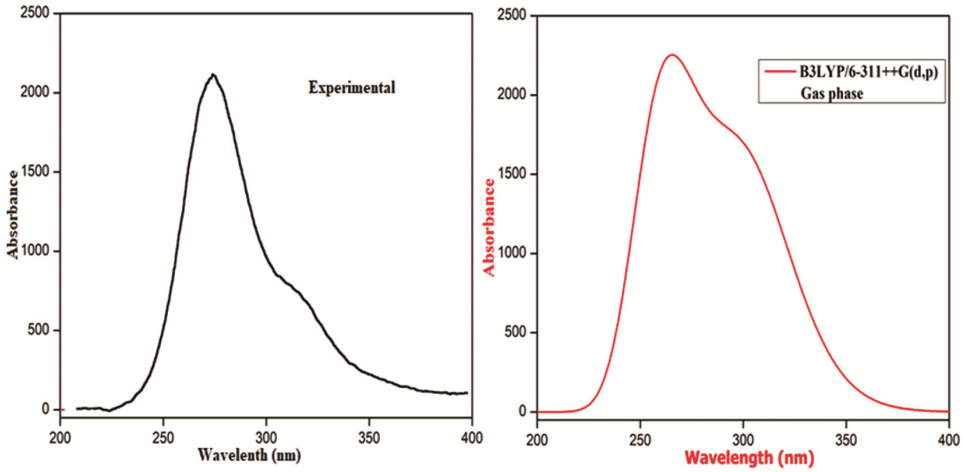

Fig.10 — UV–Vis, TD-DFT of 4B2EH

The experimental UV-visible spectra absorption 269 nm, which is the π→π* electronic transition from ground state to excited state in the 4B2EH compound, closely correlates with the electron transition 262.18 nm, excitation energy = 4.7290 eV, and oscillation strength f = 0.0503 in the current investigation. Other absorption 273.15 and 302.47 nm transitions, on the other hand, do not match the experimental values given in (Table 7), respectively. The main contribution HOMO→ LUMO (69%) found by Gauss Sum software is associated with the absorption band at 302.47 nm. Similarly, the absorption bands' wavelengths are 273.15 nm and 262.18 nm, which correspond to the title molecules' H-1->LUMO (41%) and H-2->LUMO (37%). The bandgap values of 4.0990 eV, 4.5390 eV, and 4.7290 eV were found in the following absorption spectral state, coupled with the energy values of 33060.66 cm^{-1}, 36609.50 cm^{-1}, and 38141.95 cm^{-1}. The S1, S2, and S3 gas phases showed oscillations of 0.0361 f, 0.0019 f, and 0.0503 f. The strength of the states with the highest energy contributions the modest contribution energy, H-2->LUMO (19%), HOMO->LUMO (69%), H-2->LUMO (33%), H-1->LUMO (41%), H-2->LUMO (37%), HOMO- >LUMO (15%), HOMO->L+1 (22%) and the minor Contribution energy H-5->LUMO (2%), H-1->LUMO (3%), HOMO->L+1 (18%) HOMO->LUMO (3%), H-1->LUMO (11%) H-3->LUMO (6%). In order to provide a more thorough knowledge of the material's electronic structure, Density of States (DOS) calculations were carried out to quantify the number of electronic states accessible at each energy level[44]. The density of states (DOS) is an important term in electronic structure analysis because it offers information on how electronic states are distributed across energy levels in a material[45]. Determining the contributions of various atoms and orbitals to the electronic structure helps comprehend the material's features, including conductivity, optical behaviour, and bonding properties of the 4B2EH. It explains how the distribution pattern around HOMO and LUMO is influenced by the type of acceptor moieties that remove electrons. For DOS interpretation, each structure is separated into two segments: the donor and the acceptor[46]. Gauss sum program analyses the DOS analysis data. Each component of the molecule is represented by a different color on the DOS graphs; for example, the relative intensity of the donor is displayed in green, while the relative intensity of the acceptors is indicated in red, as seen in (Fig. 11). Positive numbers on DOS graphs indicate LUMO, whereas negative values along the x-axis represent HOMO. In molecule 4B2EH, the HOMO has electron density dispersed across the molecule, with a slightly larger concentration in the donor groups[47]. On the other hand, although some electron density is linked to the donor groups, the acceptor moiety is the main source of electron density in the LUMO. The acceptor group in the LUMO exhibits a higher electron density than the donor portion. These results show that the withdrawing effect of the end-capped acceptor moieties is satisfactorily proficient.

4B2EH - NMR Analysis

Nuclear magnetic resonance (NMR) is a strong analytical technology used in physics, chemistry, biology, and medicine to examine molecular dynamics and structure. By submitting a sample to a magnetic field, NMR can identify the spatial arrangement and

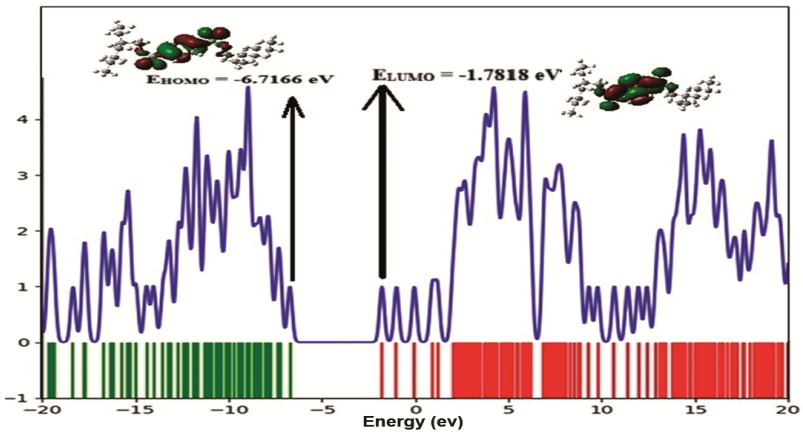

Fig. 11 — DOS state of the 4B2EH

bonding between atoms in molecules[48]. Protein structural research, chemical component detection, and medical tissue imaging can all benefit from this method. Because it is non-destructive and may yield comprehensive information on molecular surroundings, NMR is highly regarded[49]. The GIAO technique's projected chemical shifts for the title compounds' 13C and 1H NMR are displayed in the table. Because NMR reveals the groupings of hydrogen and carbon, it is useful for detecting organic compounds. To make the predictions, the B3LYP/6–311++G (d, p) approach was used[50]. The Table 8 and Figure 12 Shows how the theoretical and experimental features of the NMR shifts correspond. Higher order values of C1 with 181.10 ppm /183.75, which is a bonded with H that is present in the perfect shift of aromatic rings like the C5, C6, C2, and C4 values belong to the benzene ring of the 4B2EH compound, are contained in the C1 NMR, which contains values for the carbon shifts ranging from 189.6392 to 20.5824 ppm. C7– 98.93/99.64, C10 belong to the C-O ester group shift, and the remaining values range from 45.3191 ppm to 20.5824 ppm representing the secondary CH2 and primary CH3 groups of both ends of the Ethylhexyl group connected to the aromatic ring through the ester group.

In C22, there is a 20.5824/23.80 shift that is bonded with the H52 1.947/2.504 shift in the H1 NMR shift of the up field matched with the presence of alkyl CH groups, and the H1 contains the higher values from the H50-13.8515 to H52-1.9472. The alkyl groups of the molecule 4B2EH of uplift shifting H35 and H52 CH group are represented by the values from 1 to 3, while the downfield of CH2, CH3 groups is shown by the values from 3 to 7. Aromatic hydrogen bonds are represented by H1 values that fluctuate between 7 and 8. The shifting represents the values that correlate to the chemical 4B2EH's theoretical and experimental features based on its structural and functional conformation. The carbon (C1-C2) (C3-C4) (C5-C6) peak below 200 ppm represents the aromatic ring, which is connected to the rest of the molecule by a carbon-carbon double bond.

Docking and Ramachandra plot

Molecular docking was performed in this investigation using the Autodock 4.0 program, which predicts interactions between small compounds and a target protein's binding site and offers insights into basic biological phenomena[51]. The Protein Data Bank (PDB) provided the target protein, 2H80, 9ETE, which was downloaded in PDB format for the docking process. MolView.org was used to synthesize the ligand 4B2EH and create its structure in order to make it compatible with the PDB format[52, 53].

Table 9illustrates the significant binding affinity and binding energy of -5.08 and -5.83 kcal/mol that were found in the binding interaction between the ligand and the 2H80, 9ETE receptor shown in the (Figs. 13-15). The VAL 50 (O...HN) and ASN 48 (O…HN) link residues from the 2H80 protein have two hydrogen bonds with the C10-O11 and C7-O8 positions of 4B2EH at 2.1 Å and 2.3 Å bond distances, and their inhibition constant is 62.43 µm of RMSD 5.24 Å. With a single hydrogen bond and a 2.1 Å bond distance, the ASN 61 (O... 1HD2) bonded residues from the 9ETE protein have an inhibition constant of 68.02 µm with an RMSD of 5.03 Å. Ramachandran plot analysis, the protein's torsional angles, and the orientation of the successive residues in the protein chain are used to

Table 8 — NMR Analysis of 4B2EH

Atom	Theoretical Chemical Shift in ppm	Experimental chemical shift in ppm	Atom	Theoretical Chemical Shift in ppm	Experimental chemical shift in ppm
O_8	621.9710	-	H_{34}	10.8225	7.722
O_{11}	619.1836	-	H_{59}	10.5146	7.720
O_{12}	155.1836	-	H_{42}	10.4420	7.574
O_9	139.8976	-	H_{51}	8.3902	7.559
C_3	189.6392	193.757	H_{43}	7.6656	7.513
C_1	181.1041	183.757	H_{29}	7.6591	7.498
C_5	171.2679	172.693	H_{60}	7.6261	7.483
C_6	160.0847	159.845	H_{44}	7.2833	6.720
C_2	151.3405	157.661	H_{61}	7.2171	6.712
C_4	149.8457	156.694	H_{48}	7.0970	6.015
C_{10}	144.975	147.694	H_{65}	6.9259	6.007
C_{24}	142.206	139.428	H_{49}	6.8621	5.574
C_{16}	134.814	138.740	H_{66}	6.6379	5.467
C_7	98.9300	99.647	H_{31}	6.2844	5.106
C_{15}	45.3191	47.28	H_{32}	6.1517	4.601
C_{23}	45.2488	40.85	H_{41}	5.9134	4.371
C_{19}	36.7172	31.69	H_{58}	5.9074	4.364
C_{27}	35.9006	31.50	H_{62}	5.8444	4.353
C_{21}	29.4961	31.06	H_{57}	5.5003	4.348
C_{13}	26.2959	30.85	H_{40}	5.4148	4.336
C_{20}	25.5840	28.57	H_{46}	5.1300	4.250
C_{28}	25.0539	28.17	H_{63}	5.0171	4.243
C_{26}	24.8622	27.19	H_{45}	4.9564	4.238
C_{18}	24.8498	26.31	H_{53}	4.9441	4.231
C_{25}	21.0956	25.04	H_{36}	4.7793	3.655
C_{17}	21.0784	23.86	H_{56}	4.0041	3.589
C_{14}	20.9695	23.84	H_{39}	3.9937	3.554
C_{22}	20.5824	23.80	H_{55}	3.7411	3.512
H_{50}	13.8515	12.015	H_{54}	3.6608	3.394
H_{30}	11.2814	11.238	H_{38}	3.6452	3.172
H_{47}	11.1120	10.477	H_{37}	3.4897	2.511
H_{33}	11.0228	8.306	H_{35}	2.6895	2.507
H_{64}	10.8947	7.736	H_{52}	1.9472	2.504

determine if the ϕ\phi and ψ\psi angles of the amino acids lie within the allowed ranges[54-57]. The carboxylic acid in 4B2EH forms a dipeptide connection with the proteins amid group, exhibiting anticancer properties. The Alpha Helix area was different in 9ete and 2h80, but the Coil region was same and the Beta-sheet region was mild in the (Fig. 16). When the 2h80 and 9ete were compared, the latter's vast parallel Alpha Helix Region revealed the ligand 4B2EH's efficient binding sites. According to the docking experiments, 4B2EH has active anticancer properties.

Mathematical aspects of 4B2EH compound

A variety of degree-based topological indices on 4B2EH molecules are presented in this part to aid researchers in understanding the pertinent physical properties and chemical reactions. Molecular structures, in which each vertex is an atom and each edge is a line connecting two atoms, are used to depict drugs in theoretical chemistry. We calculated topological descriptors for the 4B2EH compound using the edge partition data. A collection of endpoints, or atoms, or vertices V (G), connected by a collection of bonds, or edges E (G), make up the molecular structure shown in the molecular graph. A molecular graph's size and order are determined by the total number of atoms, or vertices, and linkages, or edges[58]. The degree of a vertex, or the number of edges that link it, is represented by the numbers d (u) and d (v). The 4B2EH molecules are analysed in this work utilizing a range of degree-based topological markers through (Fig. 17).

Table 9 — Binding energy of 4B2EH

Protein (PDB ID)	Bonded residues	No. of hydrogen bond	Bond distance (Å)	Estimated Inhibition Constant (μm)	Binding energy (kcal/mol)	Reference RMSD (Å)
2H80	VAL 50 (O...HN) ASN 48 (O…HN)	2	2.1 2.3	62.43	-5.08	5.24
9ETE	ASN 61 (O...1HD2)	1	2.1	68.02	-5.83	5.03

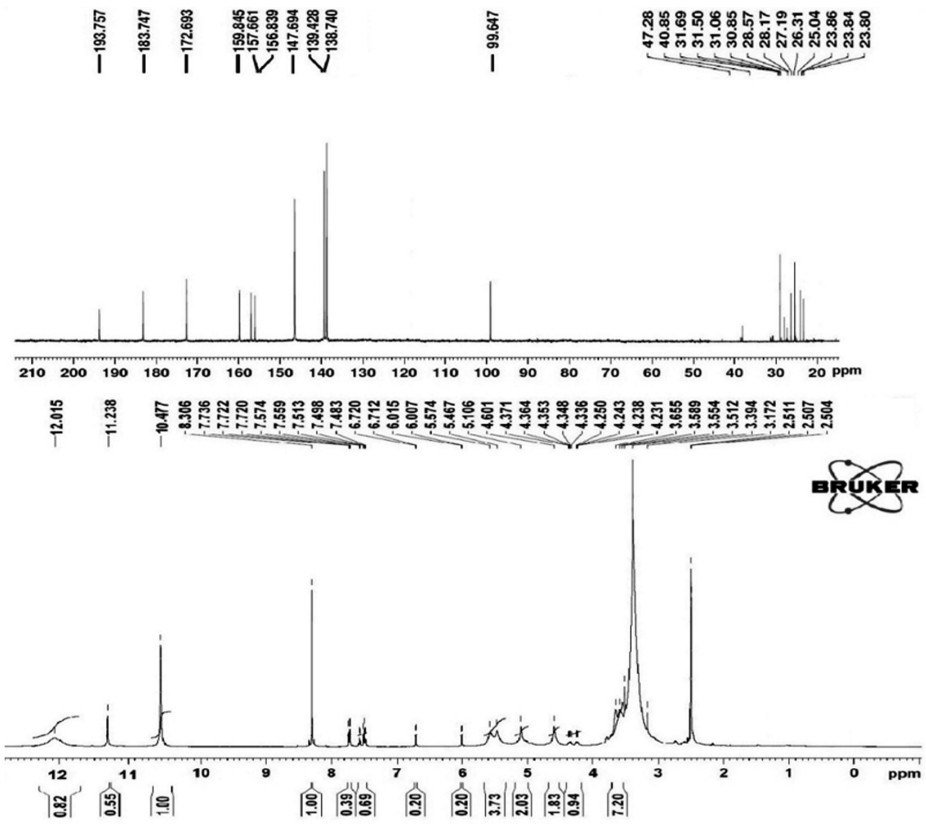

Fig.12 — NMR of H^1 and C^{13} of 4B2EH

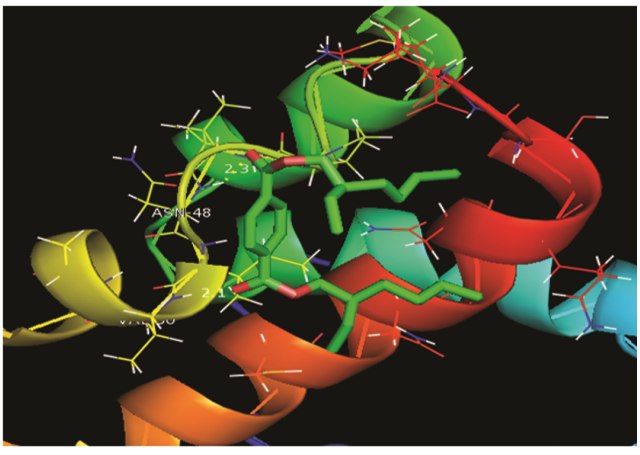

Fig.13 — Protein 2H80 Bonded residuesVAL 50 (O...HN) ASN 48 (O…HN) binding to 4B2EH

Definition 1) Trinajestic and Gutman created the first and second Zagreb indices, M1 (G) and M2 (G) [59].

$$M1(G) = \sum_{uv \in E(G)} (du + dv)$$

and

$$M2(G) = \sum_{UV \in E(G)} (du.dv)$$

Definition 2) Harmonic index H (G) is[59]commuted as

$$H(G) = \sum_{UV \in E(G)} \frac{2}{du + dv}$$

Definition 3) explains the hyper Zagreb index [59] in the following way

$$HM(G) = \sum_{uv \in E\,(G)} (du + dv)^2$$

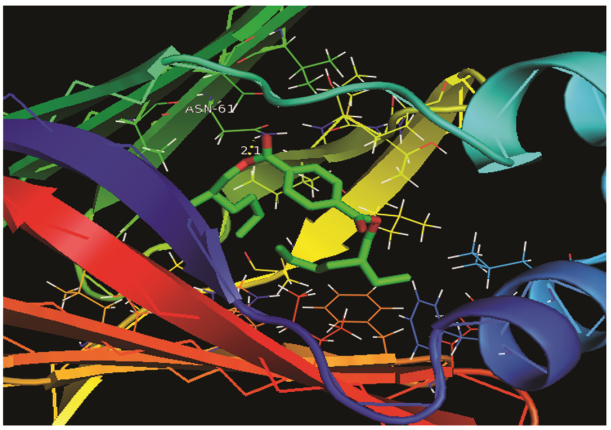

Fig.14 — Protein9ETE Bonded residues ASN 61 (O...1HD2) binding to 4B2EH

Definition 4) TheForgotten index F (G) [59] is described as

$$F(G) = \sum_{uv \in E(G)} [\,(du)^2 + (dv)^2]$$

Definition 5) The following one provides the Reciprocal Randic Index RR (G) [60] in its entirety.

$$RR(G) = \sum_{uv \in E\,(G)} \sqrt{du \times dv}$$

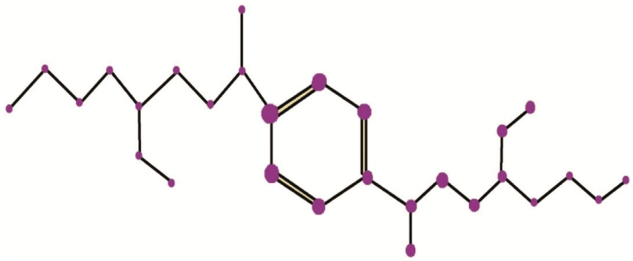

Fig.17 — Hydrogen depletion of 4B2EH

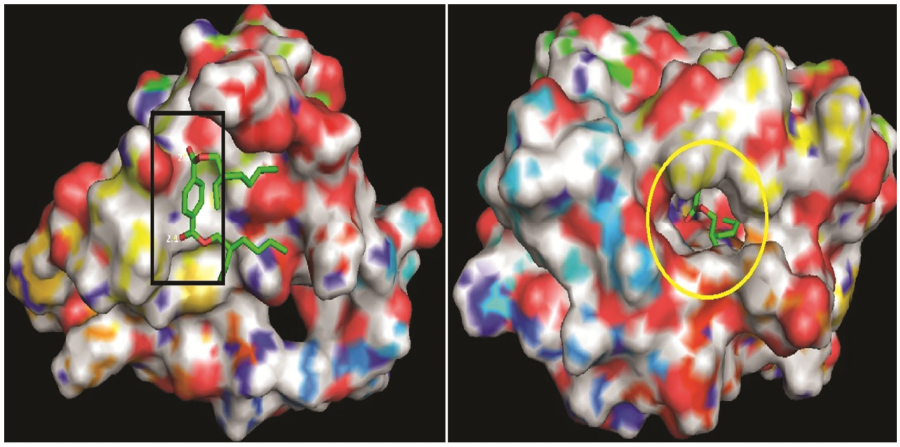

Fig.15 — 4B2EH- 3D docking

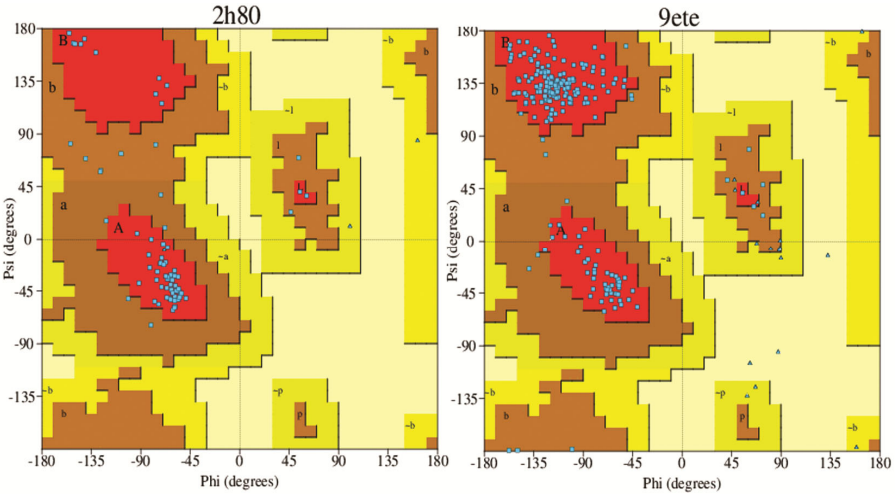

Fig.16 — 4B2EH Ramachandran plot

Table 10 — Physical and Math Comparative of 4B2EH

S. No	Physical and Chemical Properties	Physical and Chemical Properties Values	Mathematical QSPR Analytical Value.
1	Polar Surface Area	52.6Å²	58.24 RR (4B2EH)
2	Boiling Point	383°C	563 HM (4B2EH)
3	Melting Point	-48°C	-
4	Flash Point	238°C or 460 °F	291 F (4B2EH)
5	Collision Cross Section	215.81 Å²	136 M2 (4B2EH)
6	Docking RMSD	5.03 Å	5.87 RA (4B2EH)
			5.89 S (4B2EH)

Definition 6) As cited in[60], the Randicindex RA (G) is shown below.

$$RA(G) = \sum_{uv \in E\,(G)} \sqrt{\frac{1}{du \times dv}}$$

Definition 7) The Sum Connectivity S (G) [60], which is shown by

$$S(G) = \sum_{uv \in E\,(G)} \sqrt{\frac{1}{du + dv}}$$

Definition 8) Geometric-arithmetic (GA) index[60] is interpreted as

$$GA(G) = \sum_{uv \in E\,(G)} \frac{2\sqrt{du \times dv}}{du + dv}$$

Definition 9) Atom Bond Connectivity Index ABC (G) [60] is given below

$$ABC(G) = \sum_{uv \in E\,(G)} \sqrt{\frac{du + dv - 2}{du \times dv}}$$

These degree-based topological indices were found using the edge partition approaches that we acquired using the hydrogen depletion of 4B2EH (Fig. 1).

Theorem 4.12.1 If G is the molecular graph of 4B2EH molecules, then the many degree-based topological indices of G are mentioned below[61].
M1 (4B2EH) = 119, M2 (4B2EH) = 136, H (4B2EH) = 11.8, HM (4B2EH) = 563, F (4B2EH) = 291, RR (4B2EH) = 58.24, RA (4B2EH) = 5.87, S (4B2EH) = 5.89, GA (4B2EH) =25.16, ABC (4B2EH) = 22.72.

Proof: Assume that G is the 4B2EH graph and that E (i, j) is the class of edges that link vertices of degree i to degree j. From the Fig. 12 observe that $|E_{1,2}| = 4$, $|E_{2,2}| = 5$, $|E_{2,3}| = 15$, $|E_{3,3}| = 2$, $|E_{3,3}| = 3$.

i) The following is the outcome of applying Definition 1:
M1 (4B2EH) = 4 (1+2) + 5 (2+2) + 15 (2+3) +2 (3+3) = 119
and
M2 (4B2EH) = 4 (1x2) + 5 (2x2) + 15 (2x3) + 2 (3x3) = 136

ii) The following is the outcome of applying Definition 2:
H (4B2EH) = $4 \times \frac{2}{1+2} + 5 \times \frac{2}{2+2} + 15 \times \frac{2}{2+3} + 2 \times \frac{2}{3+3} = 11.8$

iii) The following is the outcome of applying Definition 3:
HM (4B2EH) = 4 x $(1+2)^2$ + 5 $(2+2)^2$ + 15 $(2+3)^2$ + 2 $(3+3)^2$ = 563

iv) The result of using Definition 4 is as follows:
F (4B2EH) = $4[1^2 + 2^2] + 5[2^2 + 2^2] + 15\,[2^2 + 3^2] + 2\,[3^2 + 4^2] = 291$

v) The result of using Definition 5 is as follows:
RR (4B2EH) = $4\sqrt{1 \times 2} + 5\sqrt{2 \times 2} + 15\sqrt{2 \times 3} + 2\sqrt{3 \times 3} = 58.24$

vi) The result of using Definition 6 is as follows:
RA (4B2EH) = $4 \times \sqrt{\frac{1}{1\times2}} + 5 \times \sqrt{\frac{1}{2\times2}} + 15\sqrt{\frac{1}{2\times3}} + 2 \times \sqrt{\frac{1}{3\times3}} = 5.87$

vii) The following is the outcome of applying Definition 7:
S (4B2EH) = $4 \times \sqrt{\frac{1}{3}} + 5 \times \sqrt{\frac{1}{4}} + 15 \times \sqrt{\frac{1}{5}} + 2 \times \sqrt{\frac{1}{6}} =$ 5.89

viii) The following is the outcome of applying Definition 8:
GA (4B2EH) = $4\left(\frac{2\sqrt{1\times2}}{1+2}\right) + 5\left(\frac{2\sqrt{2\times2}}{2+2}\right) + 15\left(\frac{2\sqrt{2\times3}}{2+3}\right) + 2\left(\frac{2\sqrt{3\times3}}{3+3}\right) 25.16$

ix) The following is the outcome of applying Definition 9:
ABC (4B2EH) = $4\sqrt{\frac{1+2-2}{1\times2}} + 5\sqrt{\frac{2+2-2}{2\times2}} + 15\sqrt{\frac{2+3-2}{2\times3}} + 2\sqrt{\frac{3+3-2}{3\times3}} = 22.72$

Table 10 explains the corresponding values of the physical and mathematical relation exhibited the

relation of it to by comparative point of view and the anticancer activity also corresponding to the values for the 5.87 RA index, 5.89 S index and the 5.03 Å RMSD value of 9ete descriptors by QSPR analysis[61].

Conclusion

The compound 4B2EH was analysed using GC-MS and DFT studies, which revealed optimized structural parameters, including maximum and minimum bond angles and bond lengths. These parameters were further supported by RDG, ELF, and LOL predictions, highlighting the electron cloud distribution and dipole moment. The bond length and angle correlations indicated the presence of non-covalent interactions and electron localization, contributing to steric effects. Using the B3LYP/6-311++G (d, p) basis set, the calculated energy gap was 5.188 eV, confirming the compound's electronic properties. The structural conformation of 4B2EH was further validated through FT-IR, UV-Vis, and NMR spectroscopy. NBO analysis identified lone pair interactions and bonding-antibonding characteristics, confirming the compound's binding nature and orientation. The FT-IR spectrum displayed broad absorption regions at 3223/3221 cm^{-1} and 3222/ 3222 cm^{-1}, indicating the presence of carbonyl groups. These functional groups played a key role in molecular docking interactions, as evidenced by electron density analysis in MEP studies. Docking studies involving the beta-sheet region of the 2H80 protein, specifically VAL 50 (O...HN) and ASN 48 (O…HN) residues, revealed binding energies of -5.83 and -5.08 kcal/mol. Lipinski's values supported the drug-likeness of 4B2EH, while molecular docking and the Ramachandran plot of the 9ETE and 2H80 proteins further confirmed its stability. Additionally, the RR (4B2EH) value of 58.24 and an RMSD value of 57.03 Å for 9ETE aligned with the mathematical descriptors from QSPR analysis, reinforcing the potential of 4B2EH as a promising liver anticancer agent.

Conflict of interest

All authors declare no conflict of interest.

References

1 Jian-Guo C, Zhu J, Yong-Hui Z, Yong-Sheng C, Lu-Lu D, Hai-Zhen C, Ai-Guo S & Gao-Ren W, Liver Cancer Survival: A Real World Observation of 45 Years with 32, 556 Cases. *J Hepatocell Carcinoma*, 8 (2021) 1023.

2 Rajsekhar PB, Bharani ARS, Angel JK, Ramachandran M & Vardhini SP, *Hybanthus enneaspermus* (L) F. Muell: A phytopharmacological review on herbal medicine. *J Chem Pharm Res*, 8 (2016) 351.

3 Fernandese MLM, Bhimrao JA, Bhandarkar A & Joshi H, Antioxidant, antiproliferative, pro-apoptotic and cell cycle arrest properties of crude extract and biofractions of *Hybanthus enneaspermus Linn*. to combat breast cancer. *RJPT*, 16 (2023) 4127.

4 Jassim L, Yunus R, Rashid U, Rashid SA, Salleh MA, Irawan S & Ghaemi F, Synthesis and optimization of 2-ethylhexyl ester as base oil for drillingfluid formulation. *Chem Eng Commun*, 203 (2016) 463.

5 Mallya R & Suvarna V, Phytochemical and Toxicity Evaluation of Methanol Extracts ofLeaves and Fruits of *Zanthoxylum rhetsa* (Rutaceae). *Biomed Pharmacol J*, 17 (2024) 1531.

6 Dhanalakshmi E, Rajesh P, Arunkumar K, Gnanasambandan T, Noureddine ISSAOUI, Sudha K & Raja M, Synthesis, GCMS, spectroscopic, electronic properties, chemical reactivity, RDG, topology and biological assessment of 1- (3, 6, 6-trimethyl-1, 6, 7, 7a-tetrahydrocyclopenta[c]pyran-yl) ethenone. *Chem Phys Impact*, 7 (2023) 100385.

7 Demir D, Tinmaz F, Dege N & Ilhan IO, Vibrational spectroscopic studies, NMR, HOMO–LUMO, NLO and NBO analysis of 1- (2-nitrobenzoyl) -3, 5-diphenyl-4, 5-dihydro-1 H -pyrazole with use X-ray diffractions and DFT calculations. *J Mol Struct*, 1108 (2016) 637.

8 Manjusha P, Prasana JC, Muthu S & Rizwana FB, Spectroscopic elucidation (FT-IR, FT-Raman and UV-visible) with NBO, NLO, ELF, LOL, drug likeness and molecular docking analysis on1- (2-ethylsulfonylethyl) -2-methyl-5-nitro-imidazole: an antiprotozoal agent. *Comput Biol Chem*, 88 (2020) 107330.

9 Medimagh M, Mleh CB, Issaoui N, Kazachenko AS, Roisnel T, Al-Dossary OM, Marouani H & Bousiakoug LG, DFT and molecular docking study of the effect of a green solvent (water and DMSO) on the structure, MEP, and FMOs of the 1-ethylpiperazine-1, 4-diium bis (hydrogenoxalate) compound. *J Mol Liq*, 369 (2023) 120851.

10 Adebiyi A, Oyeyemi S, Tedela P & Ojo VI, GC-MS Analysis of Bioactive Compounds from N-Hexane Leaf Extract of a Tropical Fern, *Nephrolepis cordifolia* (L) C. Presl. *East African Scholars J Biotechnol Genet*, 1 (2019) 118.

11 Kawai-Hirai R & Hirai M, Effect of cations on the structure of sodium bis (2-ethylhexyl) sulfosuccinate water-in-oil microemulsion. *J Appl Crystallogr*, 40 (2007) s274.

12 Li XF, Cheng D, Meng XR & Yang HX, Effects of two benzene dicarboxylic acids on the construction of CdII coordination polymers incorporating a flexible n-donor ligand. *Acta Crystallogr Sect C Struct Chem*, 75 (2019) 643.

13 Zhong H, Duan SH, Hong YP, Li ML, Liu YQ, Luo CJ, Luo QY, Xiao SZ, Xie HL, Xu YP, Yang XM, Zeng XR & Zhong QY, Erratum: Retraction of articles by H. Zhong et al. *Acta Crystallogr Sect E Struct*, 66 (2010) e11.

14 Nozad AG, Najafi H, Meftah S & Aghazadeh M, A systematic study on hydrogen bond interactions in sulfabenzamide: DFT calculations of the N-14, O-17, andH-2 NQR parameters. *Biophys Chem*, 139 (2009) 116.

15 Ramírez-Cortés SA, Durán-Vargas A, Rauda-Ceja JA, Mendoza-Espinosa P, Cofas-Vargas LF, Cruz-Rangel A, Pérez-Carreón JI & García-Hernández E, Targeting human

prostaglandin reductase 1 with Licochalcone A: Insights from molecular dynamics and covalent docking studies. *Biophys Chem*, 320 (2025) 107410.

16 Lawrence M, Rajesh P, Sahaya S & Dhas J, Quantum Chemical Calculation and Spectroscopic Approach for The Analyses Of 2-Oxovaleric Acid, Methyl Ester. *J Pharm Negat*, 13 (2022) 1495.

17 Agwupuye JA, Koudjina S, Gber TE & Zeeshand M, Benchmarking Mechanistic Structural, Molecular Docking, ADMET and Biological Properties of Methyl- Imidazole Derivatives: Potential Anti-Cancer agents. *Res Square*, (2024).

18 Vijayakumar T, Hubert Joe I, Nair CPR & Jayakumar VS, Efficient π electrons delocalization in prospective push-pull non-linear optical chromophore 4- [N, N-dimethylamino]-4′nitrostilbene (DANS): A vibrational spectroscopic study. *ChemPhys*, 343 (2008) 83.

19 Manjusha P, Johanan Christian Prasana, Muthu S & Fathima Rizwana B, Spectroscopic elucidation (FT-IR, FT-Raman and UV-visible) with NBO, NLO, ELF, LOL, drug likeness and molecular docking analysis on 1- (2-ethylsulfonylethyl) -2-methyl-5-nitro-imidazole: an antiprotozoal agent. *Comput Biol Chem*, 88 (2020) 107330.

20 Priya SY, Rao RK, Chalapathi PV, Veeraiah A, Srikanth KE, Mary SY & Thomas R, Intricate spectroscopic profiling, light harvesting studies and other quantum mechanical properties of 3-phenyl-5-isooxazolone using experimental and computational strategies. *J Mol Struct*, 1203 (2020) 127461.

21 Belaidi O, Bouchaour T & Maschke U, Molecular Structure and Vibrational Spectra of 2-Ethylhexyl Acrylate by Density Functional Theory Calculations. *Org Chem Int*, 1 (2013) 348379.

22 Breitfeld S, Scholz G, Emmerling F & Kemnitz E, BaF-benzenedicarboxylate: the first mechanochemical synthesis of a new coordination polymer with a direct Ba–F bond. *J Mater Sci*, 53 (2018) 13682.

23 Farajzadeh MA, Rahimzadeh S, Mogaddam AMR & Aghdam BMA, Fast and simple procedure for the synthesis of a zinc and 1, 4-benzene dicarboxylic acid metal-organic framework and its evaluation as a sorbent for dispersive micro solid phase extraction of pesticide residues. *RSC Adv*, 14 (2024) 28035.

24 Moreno A, Gallego-Iniesta MP, Taccone R, Martín MP, Cabañas B & Salgado MS, FTIR gas-phase kinetic study on the reactions of some acrylate esters with OH radicals and Cl atoms. *Environ Sci Pollut Res*, 21 (2014) 11541.

25 Selvakumar, JN, Chandrasekaran SD, George GPC & Kumar TD, Inhibition of the ATPase Domain of Human Topoisomerase IIa on HepG2 Cells by 1, 2-benzenedicarboxylic Acid, Mono (2-ethylhexyl) Ester: Molecular Docking and Dynamics Simulations. *Curr Cancer Drug* Targets, 19 (2019) 495.

26 Daina A, Michielin O & Zoete V, SwissADME: A free web tool to evaluate pharmacokinetics, drug-likeness and medicinal chemistry friendliness of small molecules. *Sci. Rep*, 7 (2017) 42717.

27 Lawrence M, IsacPaulraj E & Rajesh P, Spectroscopic characterization, electronic transitions and pharmacodynamic analysis of 1-Phenyl-1, 3-butanedione: An effective agent for antipsychotic activity. *Chem Phys Impact*, 6 (2023) 100226.

28 Gomathi K, Rathikha R & Rajesh P, Gas Chromatography Mass Spectroscopic, Spectral, Structural and Quantum Mechanical Studies of Behenic Acid. Int *J Mech Eng*, 7 (2022).

29 Khemalapure SS, Katti VS, Hiremath CS, Hiremath SM, Basanagouda M & Radder SB, Spectroscopic (FT-IR, FT-Raman, NMR and UV-Vis), ELF, LOL, NBO, and Fukui function investigations on (5-bromo-benzofuran-3-yl) -acetic acid hydrazide (5BBAH): Experimental and theoretical approach. *J Mol Struct*, 1196 (2019) 280-290.

30 Radder SB, Melavanki R, Hiremath SM, RavirajKusanur, Khemalapure SS & Jeyaseelan SC, Synthesis, Spectroscopic (FT-IR, FT-Raman, NMR & UV-Vis), Reactive (ELF, LOL, Fukui), Drug likeness and Molecular Docking insights onnovel4-[3- (3-methoxyphenyl) -3-oxo-propenyl]-benzonitrileby Experimental and Computational Methods. *Heliyon*, 7 (2021) e07011.

31 Swarnalatha N, Gunasekaran S, Muthu S & Rajesh P, Experimental and theoretical investigations of spectroscopic properties of acitretin. *Indian J Sci*, 14 (2017) 43-62.

32 Alam MJ, Khan AU, Alam M & Ahmad S, Spectroscopic (FTIR, FT-Raman, 1H NMR and UV–Vis) and DFT/TD-DFT studies on cholesteno [4, 6-b, c]-2′, 5′-dihydro- 1′, 5′-benzothiazepine. *J Mol Struct*, 1178 (2019) 570-582.

33 Manjusha P, Johanan Christian Prasana, Muthu S & Fathima Rizwana B, Spectroscopic elucidation (FT-IR, FT-Raman and UV-visible) with NBO, NLO, ELF, LOL, drug likeness and molecular docking analysis on 1- (2-ethylsulfonylethyl) -2-methyl-5-nitro-imidazole: an antiprotozoal agent. *Comput Biol Chem*, 88 (2020) 107330.

34 Dhanalakshmi E, Rajesh P, Arunkumar K, Gnanasambandan T, Issaoui N, Sudha K & Raja M, Synthesis, GCMS, spectroscopic, electronic properties, chemical reactivity, RDG, topology and biological assessment of 1- (3, 6, 6-trimethyl-1, 6, 7, 7a-tetrahydrocyclopenta[c]pyran-1-yl) ethenone. *Chem PhysI mpact*, 7 (2023) 100385.

35 Manjusha P, Prasana JC, Muthu S & Rizwana BF, Spectroscopic elucidation (FT-IR, FT-Raman and UV-visible) with NBO, NLO, ELF, LOL, drug likeness and molecular docking analysis on 1- (2-ethylsulfonylethyl) -2-methyl-5-nitro-imidazole: An antiprotozoal agent. *Comput Biol Chem*, 88 (2020) 107330.

36 Subbaiah S, Elangovan N, Ajithkumar G & Manoj KP, (E) -4- ((4-Bromobenzylidene) Amino) -N- (Pyrimidin-2-yl) Benzenesulfonamide from 4-Bromobenzaldehyde and Sulfadiazine, Synthesis, Spectral (FTIR, UV–Vis), Computational (DFT, HOMO–LUMO, MEP, NBO, NPA, ELF, LOL, RDG) and Molecular Docking Studies. *Polycycl Aromat Com*, 42 (2022).

37 Adindu EA, Godfrey OC, Agwupuye EI, Ekpong BO, Agurokpon DC & Ogbodo SE, Innocent Benjamin, Hitler Louis, Structural analysis, reactivity descriptors (HOMO-LUMO, ELF, NBO), effect of polar (DMSO, EtOH, H2O) solvation, and libido-enhancing potential of resveratrol by molecular docking. *Chem Phys Impact*, 7 (2023) 100296.

38 Kazachenko AS, Tanış E, Akman F, Medimagh M, Issaoui N, Al-Dossary O, Bousiakou LG, Anna S Kazachenko, Dmitry Zimonin & Andrey M Skripnikov, A Comprehensive Study of N-Butyl-1H-Benzimidazole.*Molecules*, 27 (2022) 7864.

39 Sevvanthi S, Muthu S, Aayisha S, Ramesh P & Raja M, Spectroscopic (FT-IR, FT-Raman and UV-Vis), computational

(ELF, LOL, NBO, HOMO-LUMO, Fukui, MEP) studies and molecular docking on benzodiazepine derivatives heterocyclic organic arenes. *Chem Data Collect*, 30 (2020) 100574.

40 Manjusha P, Prasana JC, Muthu S & Rizwana FB, Spectroscopic elucidation (FT-IR, FT-Raman and UV-visible) with NBO, NLO, ELF, LOL, drug likeness and molecular docking analysis on 1- (2-ethylsulfonylethyl) -2-methyl-5-nitro-imidazole: An antiprotozoal agent. *Comput Biol Chem*, 88 (2020) 107330.

41 Elangovan N, Sowrirajan S, Arumugam N, Rajeswari B, Mathew S, Priya CG & Venkatraman BR, Mahalingam SM, Theoretical Investigation on Solvents Effect in Molecular Structure (TD-DFT, MEP, HOMO-LUMO), Topological Analysis and Molecular Docking Studies of N- (5- ((4-Ethylpiperazin-1-yl) Methyl) Pyridin-2-yl) -5-Fluoro-4- (4-Fluoro-1-Isopropyl-2-Methyl-1H-Benzo[d] Imidazol-6-yl) Pyrimidin-2-Amine. *Polycycl Arom Compd*, 44 (2024) 4467.

42 Fung V, Hu G, Ganesh P & Sumpter BG, Machine learned features from density of states for accurate adsorption energy prediction. *Nat Commun*, 12 (2021) 88.

43 Hamam KJ & Alomari MI, A study of the optical band gap of zinc phthalocyanine nanoparticles using UV–Vis spectroscopy and DFT function. *Appl Nanosci*, 7 (2017) 261.

44 Khalid M, Fatima N, Arshad M, Adeel M, Braga AAC & Ahamad T, Unveiling the influence of end-capped acceptors modification on photovoltaic properties of non-fullerene fused ring compounds: a DFT/TD-DFT study. *RSC Advances*, 14 (2024) 20441.

45 Martynov AG, Mack J, May AK, Nyokong T, Gorbunova YG & Tsivadze AY, Methodological Survey of Simplified TD-DFT Methods for Fast and Accurate Interpretation of UV-Vis-NIR Spectra of Phthalocyanines. *ACS Omega*, 4 (2019) 7265.

46 Shafiq I, Khalid M, Jawaria R, Shafiq Z, MurtazaS & Braga AAC. Exploring the photovoltaic properties of naphthalene-1, 5-diamine-based functionalized materials in aprotic polar medium: a combined experimental and DFT approach. *RSC Adv*, 14 (2024) 33048.

47 Perveen M, Nazir S, Arshad AW, Khan MI, Shamim M, Ayub K, Khan MA & Iqbal J, Therapeutic potential of graphitic carbon nitride as a drug delivery system for cisplatin (anticancer drug): A DFT approach. *Biophys Chem*, 267 (2020) 106461.

48 Holland DC & Carroll AR, Structure Revision of Formyl Phloroglucinol Meroterpenoids: A Unified Approach Using NMR Fingerprinting and DFT NMR and ECD Analyses. *Molecules*, 29 (2024) 594.

49 Manwal A Mekoung P, Malloum A, Govindarajan M, Mballa RN, Patouossa I, Abouem A Zintchem, Nanseu CPN & Mbouombouo IN, Spectroscopic properties (FT-IR, NMR and UV) and DFT studies of amodiaquine. *Heliyon,* 9 (2023) 12.

50 Nardelli F, Borsacchi S, Calucci L, Carignani E, Martini F & Geppi M, Anisotropy and NMR spectroscopy. *Rendiconti Lincei Springer*, 31 (2020) 999.

51 Save SA, Lokhande RS & Chowdhary AS, Determination of 1, 2-Benzenedicarboxylic acid, bis (2-ethylhexyl) ester from the twigs of Thevetia Peruviana as a Colwell Biomarker. *J innov pharm biol sci*, 2 (2015) 349-362.

52 Selvakumar, JN, Chandrasekaran SD, George GPC & Kumar TD, Inhibition of the ATPase Domain of Human Topoisomerase IIa on HepG2 Cells by 1, 2-benzenedicarboxylic Acid, Mono (2-ethylhexyl) Ester: Molecular Docking and Dynamics Simulations. *Curr Cancer Drug Targets*, 19 (2019) 495.

53 Hisam MR, Rajesh P, Dhanalakshmi E, Laura JJ, Prabhaharan M & Jayaraman G, Topological characterization, computational, spectroscopic (FT-IR, 1H, 13C NMR) exploration, chemical reactivity analysis of 6- (3, 3-dimethyl-oxiran-2-ylidene) -5, 5-dimethyl-hex-3-en-2-one. *Next Mater*, 8 (2025) 100831.

54 Cherian A & Vadivel V, *In silico* ADME and Drug-likeness Evaluation of Phytochemicals from the Leaves of *Tabernaemontana divaricata Linn*. *Pharmacogn J*, 15 (6) (2023) 1136-1142.

55 Kekeçmuhammed H, Tapera M, Tüzün B, Akkoç S, Zorlu Y & Sarıpınar E, Synthesis, molecular docking and antiproliferative activity studies of a thiazole-based compound linked to hydrazone moiety. *Chem Select*, 7 (26) (2022) e202201502.

56 Jiang S & Bao H, Exploring the mechanism of esculetin extracted from *Chroogomphus rutilus* in treating liver cancer based on network pharmacology, molecular docking, and in vivo experimental validation. *J Ethnopharmacol*, (2025) 119837.

57 Kumar M & Rathore RS, RamPlot: a webserver to draw 2D, 3D and assorted Ramachandran (φ, ψ) maps. *J Appl Cryst*, 58 (2025) 630-636.

58 Carrascoza F, Zaric S & Silaghi-Dumitrescu R, Computational study of protein secondary structure elements: Ramachandran plots revisited. *J Mol Graph*, 50 (2014) 125.

59 Gutman I, Degree based topological indices. *Croat Chem Acta,* 86 (2013) 351.

60 Furtula B & Gutman I, A forgotton topological index. *J Math Chem*, 53 (2015) 213.

61 Gutman I, Furtula B & Elphick C, Three New/Old Vertex-Degree-Based Topological Indices. *Commun Math Comput Chem*, 72 (2014).

62 Farahani MR, On the Randic and Sum-Connectivity Index of Nanotubes. *Ann West Univ Timisoara-Mathematics Comput Sci*, 51 (2013) 39.